

Adaptive Intrinsic Plasticity in Human Dentate Gyrus Granule Cells during Temporal Lobe Epilepsy

Michael Stegen¹, Florian Kirchheim^{1,2}, Alexander Hanuschkin¹, Ori Staszewski³, Rüdiger W. Veh⁴ and Jakob Wolfart¹

¹Cellular Neurophysiology, Department of Neurosurgery, University Medical Center Freiburg, 79106 Freiburg, Germany, ²Faculty of Biology, University of Freiburg, 79104 Freiburg, Germany, ³Department of Neuropathology, University Medical Center Freiburg, 79106 Freiburg, Germany and ⁴Institute for Integrative Neuroanatomy, Charité Universitätsmedizin Berlin, 10115 Berlin, Germany

Address correspondence to Dr Jakob Wolfart, Cellular Neurophysiology, Department of Neurosurgery, University Medical Center Freiburg, Breisacher Str. 64, 79106 Freiburg, Germany. Email: jakob.wolfart@uniklinik-freiburg.de.

Granule cells in the dentate gyrus are only sparsely active in vivo and survive hippocampal sclerosis (HS) during temporal lobe epilepsy better than neighboring cells. This phenomenon could be related to intrinsic properties specifically adapted to counteract excitation. We studied the mechanisms underlying the excitability of human granule cells using acute hippocampal slices obtained during epilepsy surgery. Patch-clamp recordings were combined with pharmacology, immunocytochemistry, and computer simulations. The input resistance of granule cells correlated negatively with the duration of epilepsy and the degree of HS. Hyperpolarization-activated, ZD7288-sensitive cation (I_H , HCN) currents and highly Ba^{2+} -sensitive, inwardly rectifying K^+ (Kir) currents (and HCN1 and Kir2.2 protein) were present somatodendritically and further enhanced in patients with severe HS versus mild HS. The properties and function of I_H were characterized in granule cells. Although I_H depolarized the membrane, it strongly reduced the input resistance and shifted the current-frequency function to higher input values. The shunting influence of HCN and Kir was similar and these conductances correlated. Resonance was not observed. Simulations suggest that the combined upregulation of Kir and HCN conductances attenuates excitatory synaptic input, while stabilizing the membrane potential and responsiveness. Thus, granule cells homeostatically downscale their input-output transfer function during epilepsy.

Keywords: hippocampus neurons, homeostasis, hyperpolarization-activated cyclic nucleotide-gated (HCN) channels — h current, Kir channels, neuroprotection

Introduction

The dentate gyrus acts as a main gateway to the hippocampus, with its principal neurons, the granule cells, effectively filtering excitatory input from the entorhinal cortex. The intrinsic properties likely related to this sparsening include the relatively negative membrane potential of granule cells (Jung and McNaughton 1993), but the underlying mechanisms and their dynamics are unknown. During temporal lobe epilepsy (TLE), the hippocampus is hyperexcited and often affected by cell death and gliosis called hippocampal sclerosis (HS), in which granule cells survive better than neighboring cell types (Wyler et al. 1992; Isokawa 1996; Wuarin and Dudek 2001; Thom et al. 2002; Hsu 2007). Therefore, the mechanisms enabling granule cells to dampen excitation may become more apparent during epilepsy (Vida 2009). Indeed, recent evidence indicate that the intrinsic excitability of granule cells could be reduced during epilepsy (Stegen et al. 2009), and in

a TLE mouse model, a similar phenomenon was linked to an increased expression of inwardly rectifying K^+ (Kir) channels (Young et al. 2009). However, the underlying mechanisms for human granule cells are unclear.

Interestingly, elevated mRNA levels of hyperpolarization-activated cyclic nucleotide-gated (HCN) channels have been observed in granule cells of TLE patients with severe HS (sHS), compared with those with mild HS (mHS) (Bender et al. 2003). HCN channels mediate a mixed K^+/Na^+ current called I_H , which has important functions in the regulation of cellular rhythmogenesis and excitability of many cell types (Pape 1996; Gasparini and DiFrancesco 1997; Magee 1999; Santoro and Tibbs 1999; Berger et al. 2001; Nolan et al. 2004; Narayanan and Johnston 2007; Dyhrfeld-Johnsen et al. 2009; Hu et al. 2009). Furthermore, in several brain areas, a changed expression of HCN channels has been implicated in epileptic hyperexcitation (Brewster et al. 2002; Santoro and Baram 2003; Shah et al. 2004; Dugladze et al. 2007; Jung et al. 2007, 2010; Powell et al. 2008; Shin et al. 2008; Dyhrfeld-Johnsen et al. 2009; Huang et al. 2009; Marcelin et al. 2009; Santoro et al. 2010; Wierschke et al. 2010). However, in granule cells of the dentate gyrus, the functional role of HCN channels is far from clear, although granule cells do express HCN channels, in particular HCN1 (Stabel et al. 1992; Santoro et al. 2000; Brauer et al. 2001; Chevaleyre and Castillo 2002; Mellor et al. 2002; Notomi and Shigemoto 2004; Bender et al. 2007).

To study the mechanism underlying the regulation of granule cell excitability and to determine the function of I_H in granule cells, we conducted patch-clamp recordings in identified human granule cells of acute hippocampal slices obtained from epilepsy surgery. In addition, immunocytochemistry was conducted, and computer simulations of reconstructed human granule cells were performed. The input resistance of granule cells correlated negatively with the degree of HS and the duration of epilepsy. This phenomenon was associated with increased HCN and Kir conductances and a reduced excitability of granule cells in sHS versus mHS sections. These results point to an intrinsic plasticity that allows granule cells to effectively scale their responsiveness.

Materials and Methods

Patients

All procedures on human tissue were approved by the ethics committee of the University of Freiburg. In all cases, surgical removal of the hippocampus was clinically indicated, and written informed consent about the use in research was obtained. The responsible pathologist made the decision of which tissue could be used for research. Clinical characteristics of patients are summarized in Table 1. Patient data are based on information available in discharge letters and

Table 1

Patient data

Age OP	Sex	Age on	Seizure type	Freq.	H	AED	Additional information, syndromes	Wy
31	M	19	SP, CP	3-4	R	LT		3
61	M	39	CP, SG	4	L	CB	Depression, meningiom ^a	3
53	F	30	CP, SG	<1	L	CB, LV	Neurofibromatosis	4
32	F	2	SP, CP	10-12	L	CB, LV		3
26	F	15	SP, CP	1-2	L	TP	FCD2a	3
18	F	1	SP, CP	4	L	LT, TP		4
38	M	1	SP, CP, SG	<1	R	LT, OX	Depr.	4
38	F	29	SP, CP, SG	<1	R	CB, LV, LT	Depr., migraine	3
39	M	24	SP, CP, SG	—	R	CB, LC	Renal insufficiency, BPD	1
30	M	15	SP, CP, SG	10	R	LT	FCD1	2
27	M	1	SP, CP, SG	1	L	TP		3
47	F	15	SP, CP, SG	—	L	OX		2
15	F	3	SP, CP	5-6	L	LT, VP	FCD1b, multilobectomy ^b	2
50	F	37	SP, CP, SG	1*	R	CB	FCD1b	3
27	F	2	SP, CP, SG	50*	L	ET, LV	FCD1b	2
39	M	26	SP, CP, SG	—	R		FCD1b	3
67	F	7	SG	—	L	TP	FCD1b	4
2	M	1	SG	—	L	LT	SH/R, stroke, enceph ^c	2
27	M	25	SP, CP, SG	4*	R	CB	FCD1b	3
18	F	1	SP, CP, SG	—	R	OX, ZN	SH/L	1
17	M	8	SP, CP	3-5*	R	CL, LT	FCD1a	1
42	M	33	SP, CP, SG	8	L	OX	Hypertr. corp. amygdal ^d	2
60	M	6	SP, CP, SG	7	R	LT	FCD1b, Depr., stroke, RI	4
53	M	1	SP, CP, SG	8	L	CL, LC, LT		4
15	M	6	SP, CP, SG	2-3	R	OX, ST	SH/R, hydrocephalus	4
17	M	6	SP	—	R	LV, OX		4
31	M	18	SG	—	L	CB	FCD1b	1
14	M	5	SP, CP, SG	—	R	LT, OX	ADHD, FCD2a	2
69	M	15	SP, CP, SG	5-6	R	LV	RI, HC, gangliocyt ^e	4
22	F	10	CP, SG	5	L	LV, TP		4
46	F	2	SP, CP, SG	10	L	OX	HC, lesion ^f	4
47	F	11	SP, CP, SG	3-4	R	LC, LV		4
2	M	1	SP	2*	R	LV, TP		1
8	M	1	SP, CP, SG	8*	R	ZN		1
5	F	3	SP, CP, SG	2-3*	L	OX		2
46	F	23	CP, SG	2	L	LC	Depr., migraine	2
61	M	1	SP, CP, SG	3	R	LT, TP	FCD1b	3
55	M	16	SP, CP, SG	3	L	CB, LC, LV		4

Note: ADHD, attention deficit hyperactivity disorder; AED, antiepileptic drug; Age OP, Age on, age at hippocampus resection and epilepsy onset; BPD, borderline personality disorder; CB, carbamazepine; CL, clobazam; Depr., depression; ET, ethosuximide; FCD, focal cortical dysplasia; Freq. seizures per month; H, hemisphere; HC, hydrocephalus communicans; L, R, left, right; LC, lacosamide; LT, lamotrigine; LV, levetiracetam; OX, oxcarbazepine; RI, renal insufficiency; SH/R, SH/L, right or left spastic hemiparesis; SP, CP, SG, simple partial, complex, secondary generalized seizures; ST, sultiame; TP, topiramate; VP, valproate; Wy, Wyler grade; ZN, zonisamide; *, daily. ^aMeningiomelectomy at age 43.

^bParietal, temporal, occipital.

^cEpileptic encephalopathy.

^dHypertrophic corpus amygdaloideum.

^eGangliocytoma WHO grade I

^fLesion in gyrus frontalis medius L.

consequently may be incomplete or based on estimates. For several values of seizure frequency and duration, a mean was calculated from the available range. Duration of epilepsy was defined as the time from chronically occurring seizures to surgical removal of the hippocampus. The degree of hippocampal sclerosis (HS) of the resected hippocampi was judged by a pathologist according to the Wyler grading scheme, which estimates the degree of neuronal dropout and astrogliosis (Wyler et al. 1992). For these routine diagnostic procedures, 3- μ m transversal paraffin-embedded sections of representative areas were stained separately with hematoxylin and eosin and against glial fibrillary acidic protein, as well as neuronal nuclei. Results were grouped into those from patients with mild HS (Figs 1Aa and 2A) (Wyler grade 1-2, $n = 15$, abbreviated mHS) and severe HS (Figs 1Ab and 2G) (Wyler grade 3-4, $n = 23$, abbreviated sHS). Wyler grades 1-2 correspond to mild hippocampal damage with <10% (Wyler 1) to 10-50% (Wyler 2) neuronal dropout in pyramidal cell layers CA1, CA3, and hilus, respectively. Wyler grades 3-4, also called "classical" and "total Ammon's horn sclerosis," correspond to severe hippocampal damage with >50% neuronal dropout in CA1, CA3, and hilus and, in case of Wyler grade 4, involving damage in CA2 plus occasionally in

the dentate gyrus (Wyler et al. 1992). If HS groups were not specifically labeled, they were pooled. According to neurosurgeons, there was no systematic difference in the hippocampal resection procedure of mHS versus sHS cases (T. Freiman, personal communication).

Electrophysiology

Immediately after resection, the hippocampi were immersed in ice-cold sucrose-containing artificial cerebrospinal fluid (sucrose ACSF) containing (in mM): 87 NaCl, 25 NaHCO₃, 2.5 KCl, 1.25 NaH₂PO₄, 0.5 CaCl₂, 7 MgCl₂, 75 sucrose, and 10 glucose (equilibrated with 95% O₂/5% CO₂). Hippocampi were cut in 1-3 mm thick slices by a neuropathologist and further cut to 400 or 350 μ m with a vibratome VT1200S (Leica, Bensheim, Germany). Subsequently, slices were incubated for 30 min at 35-36 °C and thereafter kept at room temperature (RT, 22 \pm 1 °C) in oxygenated sucrose ACSF for >1 h until individual transfer for electrophysiological experiments. For somatic whole-cell patch-clamp recordings, slices were transferred to a recording chamber and continuously superfused with ACSF containing (in mM): 125 NaCl, 25 NaHCO₃, 2.5 KCl, 1.25 NaH₂PO₄, 2 CaCl₂, 1 MgCl₂, and 25 glucose (equilibrated with 95% O₂/5% CO₂). Experiments were conducted at RT except resonance recordings (see below). Cells were visualized by infrared Dodt gradient contrast video microscopy (Luigs and Neumann, Ratingen, Germany) using a $\times 63/1.0$ objective in an upright microscope (Axioskop2 FS, Zeiss, Oberkochen, Germany). Patch pipettes (2.0 mm OD, 1.0 mm ID, Hilgenberg, Malsfeld, Germany) were pulled from borosilicate glass using a DMZ-universal puller (Zeitz, Martinsried, Germany). Pipettes were filled with a solution containing (in mM): 135 K gluconate, 20 KCl, 10 4-(2-hydroxyethyl)-1-piperazineethanesulfonic acid (HEPES), 0.1 ethyleneglycol-bis(2-aminoethylether)-N,N,N',N'-tetra acetic acid (EGTA), 2 MgCl₂, 2 Na₂ATP, and 0.2% biocytin (adjusted to pH = 7.28 with KOH) and had tip resistances of 5.2 \pm 0.1 M Ω . The liquid junction potential was determined to be 10 mV, and voltages were appropriately corrected offline. Series resistances (R_{ser} , 11.6 \pm 0.2 M Ω) were compensated via bridge balance, and pipette capacitance was compensated. Seal resistances (R_{seal}) were >1 G Ω (3.4 \pm 0.2 G Ω ; see results for R_{ser} and R_{seal} group comparisons). Artificial excitatory postsynaptic currents (α EPSCs) were created with an alpha function

$$I(t) = A e^{-\frac{t}{\tau}} e^{1-\frac{t}{\tau}}$$

where A is an adjusting factor for the peak current, and τ (2.5 ms) the time of the peak. Membrane resonance was tested using the impedance (Z) amplitude profile (ZAP) method (Hu et al. 2009): small currents (less than ± 50 pA) with linearly increasing frequency (0-15 Hz for 30 s) according to the sinusoidal function

$$I(t) = A \sin\left(\frac{(f_0 + (f_1 - f_0))\pi t^2}{t_1}\right),$$

were injected to evoke subthreshold voltage oscillations ($< \pm 10$ mV, ZAP analysis see below); A is an adjusting factor for the peak current, f_0 and f_1 are minimal and maximal frequencies respectively and t_1 refers to the time point where f_1 is reached. This subset of experiments was conducted at 34.3 \pm 0.2 °C ($n = 12$); the starting voltage was adjusted to -90.0 \pm 0.1 mV. Electrophysiological recordings were filtered at 5-20 kHz using a SEC05LX amplifier (NPI, Tamm, Germany) and digitized at 10-40 kHz (voltage and current clamp, respectively) using an ITC18 D/A converter (Instrutech, Port Washington, NY) and the software PatchMaster (Heka, Lambrecht, Germany). To obtain optimal biocytin-labeling, the whole-cell configuration was maintained for at least 30 min, and the pipette was retrieved via the outside-out configuration.

Pharmacology

When mentioned, experiments were conducted in the presence of inhibitors of AMPA/kainate-type and NMDA-type glutamate receptors as well as γ -aminobutyric acid (GABA)-A receptors using 50 μ M D(-)-2-amino-5-phosphonopentanoic acid (D-AP5), 20 μ M 1,2,3,4-tetrahydro-7-nitro-2,3-dioxoquinoxaline-6-carbonitrile disodium (CNQX), and 100 μ M picrotoxin (PTX), respectively. For inhibition of fast sodium

channels, we used tetrodotoxin (TTX, 0.5 μ M). The following drugs were kept in H₂O stocks at -20 °C: D-AP5, CNQX, TTX, BaCl₂, 4-ethylphenylamino-1,2-dimethyl-6-methylaminopyrimidinium chloride (ZD7288, abbreviated "ZD"). PTX was kept in DMSO stocks at -20 °C. Before experiments, stocks were diluted (1:1000) in oxygenated glucose ACSF. Drugs were kept in glass syringes of an application system (AutoMate Scientific, Berkeley, CA) under carbogen pressurized at 1.3-1.6 bar before bath application. We obtained D-AP5, CNQX, and TTX from Ascent Scientific (Weston-Super-Mare, UK) and all other substances from Sigma-Aldrich (Munich, Germany). At least 7 different batches of ZD were used (Ascent Scientific and Tocris, Bristol, UK).

Morphology and Cell Type Identification

After recording, slices were fixed overnight with 4% paraformaldehyde in 0.1 M phosphate buffer (PB, pH 7.4). After 3 washing steps with PB, slices were treated for 30 min with a blocking solution containing 0.3% Triton X-100 and 10% normal goat serum (NGS, Vector Laboratories, Burlingame, CA) and incubated either for >3 h at RT or overnight at 4 °C with a rabbit polyclonal anti-Prox1 antibody (1:1000, Chemicon, Temecula, CA) in 0.1% Triton and 1% NGS. After 3 washes, slices were incubated with Alexa Fluor-546-Streptavidin (1:500, Invitrogen, Karlsruhe, Germany) or AvidinD-Fluorescein FITC (1:500, Vector Laboratories) for biotin detection and a secondary anti-rabbit antibody conjugated with Alexa Fluor-488 (1:200, Invitrogen) either for >3 h at RT or overnight at 4 °C. After 5 washes, slices were mounted in fluorescence mounting medium (DAKO, Glostrup, Denmark) or ProLong gold antifade reagent (Invitrogen). For overview reconstructions and cell identification, immunofluorescence was analyzed with an Axioplan 2 microscope equipped with Apotome technology (Zeiss) using the $\times 20/0.75$ objective and extended focal images.

Immunoperoxidase Histochemistry

To map the HCN1 and Kir2.2 channel distribution in the human hippocampus, resected human hippocampi were cut to 2-3 mm transversal blocks and fixed in 4% PFA for 4 h. Samples were rinsed with water, dehydrated in EtOH (90 min in 70%, 80%, 96%, respectively plus 3 \times 1 h in 100%), in xylol (2 \times 60 min), incubated twice in paraffin (60 min, 60 °C), and solidified. Paraffin-embedded hippocampi were cut to 3- μ m thick slices on a microtome (HM 360, Microm, Walldorf, Germany) and mounted on glass slides (superfrost plus, Langenbrink, Emmendingen, Germany). Excess paraffin was removed by incubation during 30 min at 85 °C, and dried sections were stored until use. For immunocytochemistry, paraffin was removed by xylol-incubation (3 \times 10 min) and sections were rehydrated twice for 2 min in EtOH (100%, 96%, 70%), rinsed in water and, without intermediate drying, covered with a few drops of 10% NGS (Interchem, Bad Kreuznach, Germany) in phosphate buffered saline (PBS) at pH 7.4 for 30 min at RT. Primary antibodies were diluted (HCN1, 1:100, Chemicon; Kir2.2, 1:100; [Pruss et al. 2003]) in PBS containing 10% NGS, 0.3% Triton X-100, and 0.1% sodium azide, and applied overnight at RT. After thoroughly rinsing with PBS and pretreatment for 1 h with 0.2% bovine serum albumine in PBS (PBS-A), sections were incubated for 4 h in secondary antibody (biotinylated goat-anti-rabbit IgG, 1:2000; Vector Laboratories). After repeated washings in PBS and preincubation for 1 h in PBS-A, the biotinylated secondary antibodies in the sections were complexed for another 2 h with a preformed ABC-complex (Vector Laboratories, 1:200 in PBS-A). After further thorough rinses in PBS, preincubation for 15 min in a solution of 0.05% diaminobenzidine and 10 mM imidazole in 50 mM Tris buffer, pH 7.6, the visualization of the antigen-antibody complexes was started by adding the same solution, complemented with ammonium nickel sulfate and hydrogen peroxide at final concentrations of 0.3% and 0.0015%, respectively. The reaction was stopped after 15 min at RT by repeated washings with PBS. Sections were dehydrated through a graded series of ethanol, transferred to xylol and coverslipped with Entellan (Merck, Darmstadt, Germany). For Nissl-staining, sections were rinsed in bidistilled water and incubated with 0.2% cresyl violet acetate in 20 mM acetate buffer, pH 4.0, for 30 min at RT. After short rinses in bidistilled water, sections were dehydrated as above and coverslipped in Entellan.

Cell Reconstruction and Computer Simulations

For detailed morphological reconstructions, optical sections of FITC-positive cells were obtained with a FluoView1000 confocal microscope (Olympus, Hamburg, Germany) equipped with a multiline argon laser (488 nm for FITC detection), a helium-neon green laser (543 nm for Cy3 detection) and a $\times 20/0.95$ (or $\times 25/1.05$) water immersion objective. The software FluoView FV10 ASW 2.0 was used to obtain images stacks (1600 \times 1600 pixels in *x-y* plane and 0.6 μ m in *z*-axis) which were either merged to 2D for figures or saved as tiff stacks. For reconstructions, tiff stacks were deconvolved using the software Huygens Professional (Scientific Volume Imaging BV, Hilversum, The Netherlands). Cells were manually traced using the software NeuronStudio (Rodriguez et al. 2008), and their morphological data were imported to the software NEURON 7.1 for Linux (<http://www.neuron.yale.edu>) that was used for simulations. Spines were modeled as consisting of a head with measured size and a neck with variable length and fixed diameter of 0.18 μ m. The integration time step for all simulations was 25 μ s. For fitting, the built-in "Brent's principal axis" algorithm to minimize the sum of squared errors (χ^2) was used. The specific membrane resistance (R_m) and intracellular resistivity (R_a) were obtained by fitting a passive model to 300 ms of the experimentally recorded voltage response to 10 pA (mHS cell: R_{in} , 299 M Ω , τ_m , 42 ms; mHS model: R_a , 142.03 $\Omega \cdot$ cm, R_m , 42.36 k $\Omega \cdot$ cm²; sHS cell: R_{in} , 80 M Ω , τ_m , 15 ms; sHS model: R_a , 212.56 $\Omega \cdot$ cm, R_m , 14.79 k $\Omega \cdot$ cm²). Membrane capacitance (C_m) was fixed at 1.0 μ F/cm², close to previously determined values (Schmidt-Hieber et al. 2007). Conductance-based models were obtained by implementing an HCN conductance (g_{HCN}) (Li and Ascoli 2006) and a Kir2 conductance (g_{Kir}) (Steephen and Manchanda 2009). These conductances were homogeneously distributed over all segments. The Hodgkin-Huxley equation for the equivalent circuit of a membrane segment is given by

$$C_m \dot{V} = I - g_{pas}(V - E_{pas}) - \bar{g}_{HCN} m_{HCN}(V - E_{HCN}) - \bar{g}_{Kir} m_{Kir}(V - E_{Kir}),$$

where g_{pas} is the passive conductance, \bar{g}_i is the maximal conductance of channel type i , and E_i is the reversal potential ($E_{HCN} = -41.9$ mV; $E_{Kir} = -105$ mV; E_{pas} was used as free parameter in fits). The activation gate variables m_i are defined by:

$$m_i = \frac{m_{\infty,i} - m_i}{\tau_i}$$

The steady state $m_{\infty,i}$ is described by the Boltzman equation:

$$m_{\infty,i}(V) = \frac{1}{1 + e^{(V_{50,i} - V)/k_i}},$$

where $V_{50,i}$ is the midpoint potential and k_i is the slope. Following Moroni et al. (2000), the time constants (and their voltage dependence) of HCN and Kir channels were modeled by:

$$\tau_i(V) = \frac{1}{a e^{-V/V_{0,i}} + b e^{V/V_{0,i}}},$$

where the denominator is the sum over opening and closing rates. For the HCN conductance of the mHS model, $m_{\infty,HCN}$ was calculated from the steady state I/V of ZD-sensitive currents measured in the respective mHS cell ($V_{50,HCN} = -73.8$ mV, $k_{HCN} = -8.8$ mV), while τ_{HCN} was calculated from mean fast τ_{HCN} values of pooled ZD-sensitive currents of mHS cells (see Results). For the Kir conductance of the mHS model, $m_{\infty,Kir}$ was determined by fitting $V_{50,Kir}$ to 3 hyperpolarizing voltage responses and fixing k_{Kir} ($V_{50,Kir} = -107.6$ mV, $k_{Kir} = -10.0$ mV). The τ_{Kir} function of the mHS model was calculated from τ_{Kir} values of Ba²⁺-sensitive currents measured in a representative mHS cell ($V_{0,Kir} = 67.08$ mV, $a = 6.1$ s⁻¹, $b = 8.1$ s⁻¹). These HCN and Kir parameters were kept constant for the sHS model. The g_{HCN}^- of the models was adjusted to fit the experimentally measured ZD-sensitive g_{rest} (at -80 mV) of the 2 respective cells (\bar{g}_{HCN} : mHS, 1.76×10^{-5} S/cm²; sHS, 2.63×10^{-5} S/cm²). The \bar{g}_{Kir} was estimated via the Ba²⁺-sensitive current of the mHS cell (\bar{g}_{Kir} , 9.10×10^{-5} S/cm²) for the mHS model and fitted for the sHS model (\bar{g}_{Kir} , 2.17×10^{-4} S/cm²). In addition, a g_{pas} was implemented to fit the voltage responses (mHS, g_{pas} , 1.10×10^{-5} S/cm², E_{pas} , -105.9 mV; sHS, g_{pas} , 2.67×10^{-5} S/cm², E_{pas} , -105.2 mV). Membrane resonance was evaluated using the ZAP method described above (starting value -95 mV, amplitude 1 mV), and the Q value described below. The α EPSCs were

simulated injecting currents described by the alpha function (starting voltage -100 mV) into distal dendrites at similar distance from the soma (mHS, 485 μm ; sHS, 479 μm).

Data Analysis

Electrophysiological records were analyzed using IgorPro (WaveMetrics, Portland, OR) and FitMaster (Heka). The viability of recorded cells was judged by a combination of electrophysiological and morphological criteria: only cells located in the granule cell layer, with granule cell-typical morphology, a resting membrane potential (V_{rest}) negative to -60 mV, and overshooting action potentials (mean peak 37.3 ± 0.9 mV) were included in the analysis. The “passive” properties of granule cells were measured at the beginning of every whole-cell recording (in ACSF and at RT) as follows. The V_{rest} was averaged from a -25 s trace. Cell capacitance (C) was obtained from the integral of the capacitive transient from -4 mV steps (50 traces averaged). Membrane time constant (τ_m) was the slow component of a double exponential fit to the average of 25 voltage responses (<5 mV) to square current pulses. Cellular input resistance (R_{in}) was calculated from the slope of the steady state current-voltage relation with voltage responses of less than ± 10 mV from V_{rest} . The “resting conductance” (g_{rest}) was measured as the ratio of the voltage response to one small negative current injection (4 steps of 3 mV from a holding potential of -80 mV) and normalized to C (g_{rest} density). The rheobase was defined as the minimal current necessary to evoke at least one action potential within 1 s using small current step differences (5 to 10 pA). The current sensitive to 50 μM ZD (I_{H}) was calculated by subtracting current traces before and after ZD application. Activation and deactivation time constants were fitted to a double exponential equation accepting only amplitudes >5 pA. Voltage dependence of activation was determined by stepwise hyperpolarization and fitting of normalized current amplitudes to the Boltzman equation (see above). Voltage dependence of activation and deactivation time constants were fitted to a double exponential function (see above). The reversal potential (V_{rev}) of I_{H} was determined by measuring the ZD-sensitive tail current amplitude 20 ms after hyperpolarization to -130 mV and linearly extrapolating to 0 mV. The permeability ratio of Na^+/K^+ was calculated applying the Goldman-Hodgkin-Katz equation

$$\frac{P_{\text{Na}}}{P_{\text{K}}} = - \left(\frac{c_{\text{K},\text{o}} - c_{\text{K},\text{i}} e^{V_{\text{rev}}/RT}}{c_{\text{Na},\text{o}} - c_{\text{Na},\text{i}} e^{V_{\text{rev}}/RT}} \right),$$

where P is permeability, c concentration (o, outer; i, inner), F , Faraday constant, R , gas constant, and T , temperature. Membrane resonance was evaluated by subjecting current and voltage traces to fast Fourier transformations. The Z value was obtained by dividing the transformed voltage by the transformed current. Resonance was quantified via the “ Q value” which was obtained by dividing the peak of the Z profile by the peak at 1.00 ± 0.30 Hz (in the model) or the mean Z value at 1.00 ± 0.038 Hz (in experiments) (Hu et al. 2009). Spontaneous EPSCs were evaluated by calculating the mean EPSC charge of a 3-min trace, using the software MiniAnalysis (Synaptosoft, Decatur, GA). Statistical significance of group differences was measured using the software Prism 4.0 (GraphPad, San Diego, CA) applying the following tests: Mann-Whitney’s test for 2 groups not normally distributed, Students t -tests for 2 groups normally distributed. The Shapiro-Wilk normality test was used to verify normal distribution. Significance of correlation was determined according to a table of Pearson’s r -values. Levels of significance are indicated in figures as * (<0.05), ** (<0.01), and *** (<0.001). The arithmetic mean values contained in the text are \pm standard error of the mean and numbers represent cells if not mentioned otherwise. Box plots display median with 25th/75th percentiles (upper and lower quartiles) and maximal/minimal values (whiskers), respectively. Figures were produced using Prism (GraphPad) and Adobe Creative Suite 3 (München, Germany).

Results

HCN and Kir Resting Conductances in Granule Cells of TLE Patients with mHS and sHS

We recorded 102 neurons in the dentate gyrus of resected hippocampi from 38 TLE patients (Table 1 and Fig. 1). To

ensure that these neurons were granule cells, they were filled with biocytin during the recording for post hoc morphological characterization and additionally stained with the granule cell marker Prox1 (Liu et al. 2000) for immunocytochemical identification (Fig. 1A, insets). At the beginning of each recording, the viability of the cells was verified and their passive properties were determined (Fig. 1B; see Materials and Methods). Overall, the morphological and electrophysiological properties were in the range of those previously described for human granule cells recorded using the patch-clamp technique in acute tissue slices (Williamson et al. 1995; Isokawa 1996; Selke et al. 2006; Williamson and Patrylo 2007; Stegen et al. 2009). Recorded cells were grouped into those from patients with mild and severe hippocampal sclerosis (mHS, Figs 1Aa and 2A; sHS, Figs 1Ab and 2G, respectively; for quantification of sclerosis, see Materials and Methods).

The mean input resistance (R_{in}) and membrane time constant (τ_m) values were reduced in sHS versus mHS cells, in other words, sHS cells were “leakier” than mHS cells (Fig. 1B) (R_{in} : mHS 350.3 ± 24.4 M Ω , $n = 39$, sHS 221.4 ± 14.2 M Ω , $n = 51$, $P < 0.001$; τ_m : mHS, 43.2 ± 2.1 ms; sHS 28.4 ± 1.2 ms, $P < 0.001$), consistent with previous observations (Stegen et al. 2009; Young et al. 2009). Pooling the data of the present and a previous study (Stegen et al. 2009), the R_{in} correlated with the Wyler grade of HS (not shown, $r = 0.34$, $n = 139$, $P < 0.001$). The resting membrane potentials (V_{rest}) of mHS and sHS cells were in a similar range, but the mean was slightly hyperpolarized in the latter (mHS, -73.1 ± 1.0 mV, $n = 39$; sHS, -78.9 ± 0.9 mV, $n = 51$; $P < 0.001$). The cell capacitances (C) of mHS and sHS cells were not different (mHS, 93.9 ± 4.3 pF, $n = 39$; sHS, 98.9 ± 5.2 pF, $n = 51$; $P = 0.5$) suggesting that overall, mHS and sHS cells were not different in size (see below).

During negative current injections, granule cells responded with an initial hyperpolarization followed by a “sag-like” depolarization (Fig. 1C), the typical hallmark of cells expressing HCN channels (Pape 1996). Application of the HCN channel inhibitor ZD7288 (50 μM , ZD) (Gasparini and DiFrancesco 1997) abolished or reduced the sag response (Fig. 1C, $n = 18$), demonstrating that granule cells possess functional HCN channels.

As previous studies showed conflicting data about R_{in} differences in mHS and sHS granule cells (Williamson et al. 1995; Isokawa 1996; Selke et al. 2006; Stegen et al. 2009), a systematic bias in the recording conditions may be responsible for the measured differences. However, we did not detect a difference in seal resistance (R_{seal}) or series resistances (R_{ser}) between the 2 compared groups (R_{seal} : mHS, 3.78 ± 0.41 G Ω , $n = 37$; sHS, 3.07 ± 0.31 G Ω , $n = 49$, $P = 0.13$; R_{ser} : mHS, 12.2 ± 0.3 M Ω , $n = 32$; sHS, 11.7 ± 0.3 M Ω , $n = 48$, $P = 0.35$). In addition, the ratio between R_{in} and R_{seal} was below 0.3 and was similar between the groups ($R_{\text{in}}/R_{\text{seal}}$: mHS, 0.12 ± 0.01 , $n = 37$; sHS, 0.10 ± 0.01 , $n = 49$, $P = 0.22$).

A reduction in R_{in} could be due to a decrease in specific membrane resistance (R_m) and/or due to an increase in membrane surface. The τ_m can be used as a direct estimate of R_m because it is the product of R_m and the specific membrane capacitance (C_m), which displays only little variations in granule cell membranes (Schmidt-Hieber et al. 2007). As τ_m was reduced in sHS granule cells, our results suggest that cell size was not responsible for the difference in R_{in} . To reaffirm this result and to estimate the relation between R_{in} and size of human granule cells, we quantified the membrane surface of a subset of recorded granule cells using detailed 3D reconstructions of confocal image stacks (see

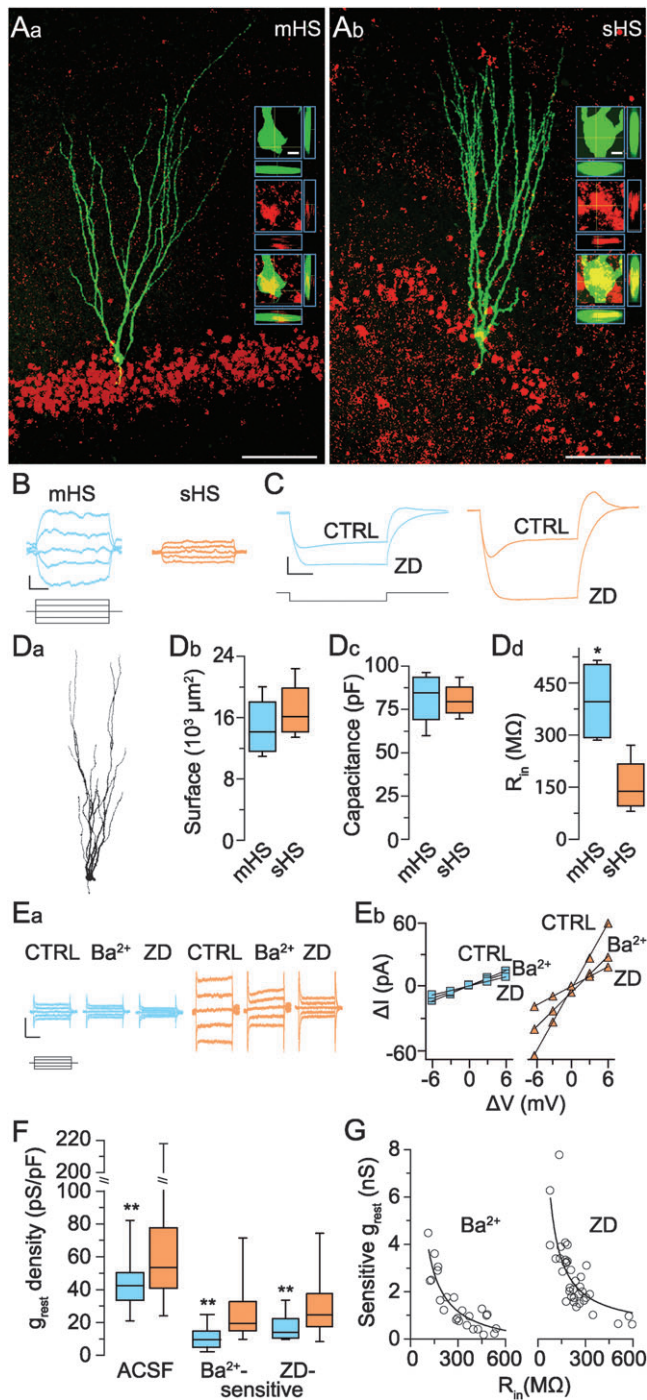


Figure 1. (A) Dentate gyrus granule cells from TLE patients with mild and severe hippocampal sclerosis (Aa, mHS; Ab, sHS, respectively). During recordings, cells were labeled with biocytin (green) and post hoc processed for immunocytochemistry and confocal reconstruction. Note typical dispersion of granule cell layer in the sHS case (Ab, compare also Fig. 2). Red, granule cell marker Prox1. Scale bars, 100 μm . Insets, magnified 3D view of somata displaying double labeling of Prox1 and biocytin (scale bar, 5 μm ; side panels with z-axis view were compressed by 36%). (B) Reduced voltage responses of sHS (orange, right traces) compared with mHS (blue, left traces) cells, with equal current injections (square pulses below, steps of 5 pA, from +10 to -10 pA). Scale bars, 1 mV, 0.2 s. (C) Hyperpolarization evoked sag-like depolarizations (CTRL, control) were inhibited by HCN channel blocker ZD7288 (ZD, 50 μM). Note larger effect of ZD in sHS cells. Scale bars, 10 mV, 0.2 s. Current step, -100 pA in all cases. (D) Morphological quantification from confocal reconstructions (Da) of a subset of cells. While membrane surface (Db) and capacitance (Dc) were similar in these mHS and sHS cells ($n = 4$, respectively), the input resistance (R_{in}) was also reduced in this sHS subset (Dd). (E) The resting conductance (g_{rest} density) was determined via small current responses (Ea) evoked from -80 mV (black lower traces, steps ± 3 mV) and fitting the slope of I/V relations (Eb). Note larger currents in sHS versus mHS granule cells (orange and blue CTRL traces, respectively). Scale bars, 40 pA, 0.2 s. (F) Mean g_{rest} densities sensitive to 200 μM Ba²⁺ or ZD. Both, the Ba²⁺- and the ZD-sensitive g_{rest} densities were enlarged in sHS versus mHS cells. Only ZD-sensitive values without prior Ba²⁺ application were included for this analysis (CTRL: mHS, $n = 37$, sHS, $n = 49$; Ba²⁺: mHS, $n = 15$, sHS, $n = 13$; ZD: mHS, $n = 11$, sHS, $n = 26$). (G) The g_{rest} sensitive to Ba²⁺ or ZD correlated with the R_{in} of the respective cells in a hyperbolic manner (mHS and sHS cells pooled), indicating that both conductances are involved in controlling the R_{in} of human granule cells.

Materials and Methods, Fig. 1Da,Db). In addition, the cell capacitance, which is commonly used to estimate the surface, was plotted for these cells (Fig. 1Dc). The total membrane surface and the capacitance of mHS and sHS cells were in a similar range (Fig. 1Db,Dc) (surface: mHS, $14\,860 \pm 2040 \mu\text{m}^2$, $n = 4$; sHS, $17\,030 \pm 1970 \mu\text{m}^2$, $n = 4$; $P = 0.49$; capacitance: mHS, 81.2 ± 8.1 pF, $n = 4$; sHS, 80.3 ± 5.1 pF, $n = 4$; $P = 0.89$). In the same cells, the R_{in} was significantly lower in the sHS compared with the mHS subset (Fig. 1Dd) (R_{in} : mHS, 394.8 ± 60.2 M Ω , $n = 4$; sHS, 155.5 ± 41.4 M Ω , $n = 4$; $P < 0.05$). Nevertheless, as R_{in} is related to cell size, we normalized conductances to capacitance in the following. The results thus far suggest that the reduced R_{in} of sHS granule cells was not due to a recording artifact or an increased membrane surface but instead due to increased membrane conductivity.

To compare the resting conductances of human granule cells in a more controlled manner, we measured the resting conductance (g_{rest}), that is, the slope of the voltage-current relationship recorded with small voltage commands close to -80 mV (Fig. 1Ea,Eb). Consistent with the difference in R_{in} , the total g_{rest} density in ACSF was increased in sHS versus mHS cells (Fig. 1E,F) (total g_{rest} density: mHS, 42.8 ± 2.2 pS/pF, $n = 37$; sHS, 65.4 ± 5.5 pS/pF, $n = 49$; $P < 0.01$). This difference was also present in the absolute values (mHS, 4.0 ± 0.3 nS, $n = 37$; sHS, 6.1 ± 0.5 nS, $n = 49$; $P < 0.001$). Sequential application of 200 μM Ba²⁺ and 50 μM ZD both reduced the g_{rest} (Fig. 1E, see also Fig. 3A), suggesting that HCN channels (Gasparini and DiFrancesco 1997) and an inwardly rectifying K⁺ (Kir) conductance (Coetzee et al. 1999) contributed to the g_{rest} of human granule cells. The Ba²⁺ inhibition of g_{rest} showed a steep concentration dependency (not shown). The Ba²⁺-sensitivity and inward rectification of these currents in human and mouse granule cells (Stegen et al. 2009; Young et al. 2009) suggests that the Kir conductance is at least in part mediated by Kir2 subtype channels. No further molecular identification of this conductance was attempted here; instead, the current sensitive to 200 μM Ba²⁺ was functionally defined as "Kir current". Simultaneous application of Ba²⁺ and ZD resulted in the occlusion of g_{rest} differences between mHS and sHS cells (g_{rest} density: mHS, 18.4 ± 3.3 pS/pF, $n = 15$; sHS, 34.1 ± 8.3 pS/pF, $n = 13$; $P = 0.15$), indicating that Kir and HCN channels were the main contributors to the conductance difference. We have no indication that tonic GABA-A or persistent Na⁺ currents contributed to the conductance difference since the g_{rest} was similar before and after the application of picrotoxin and TTX (g_{rest} density: ACSF, 58.2 ± 10.1 pS/pF, $n = 6$; PTX/TTX, 56.8 ± 10.8 pS/pF, $n = 6$; $P = 0.69$).

To quantify the effects of Ba²⁺ and ZD, we subtracted traces before and after drug application. Only one drug per experiment was applied in these cases. The Ba²⁺-sensitive (Ba²⁺-sens.) g_{rest} was prominent, and it was enlarged on average in sHS compared with mHS cells (Fig. 1E,F) (Ba²⁺-sensitive g_{rest} density:

was determined via small current responses (Ea) evoked from -80 mV (black lower traces, steps ± 3 mV) and fitting the slope of I/V relations (Eb). Note larger currents in sHS versus mHS granule cells (orange and blue CTRL traces, respectively). Scale bars, 40 pA, 0.2 s. (F) Mean g_{rest} densities sensitive to 200 μM Ba²⁺ or ZD. Both, the Ba²⁺- and the ZD-sensitive g_{rest} densities were enlarged in sHS versus mHS cells. Only ZD-sensitive values without prior Ba²⁺ application were included for this analysis (CTRL: mHS, $n = 37$, sHS, $n = 49$; Ba²⁺: mHS, $n = 15$, sHS, $n = 13$; ZD: mHS, $n = 11$, sHS, $n = 26$). (G) The g_{rest} sensitive to Ba²⁺ or ZD correlated with the R_{in} of the respective cells in a hyperbolic manner (mHS and sHS cells pooled), indicating that both conductances are involved in controlling the R_{in} of human granule cells.

mHS, 10.7 ± 1.7 pS/pF, $n = 15$; sHS, 27.0 ± 5.0 pS/pF, $n = 13$; $P < 0.01$). Similarly, the ZD-sensitive g_{rest} was notable and increased in sHS versus mHS cells (Fig. 1E,F) (ZD-sensitive g_{rest} density: mHS, 17.8 ± 2.3 pS/pF, $n = 11$; sHS, 29.2 ± 2.8 pS/pF, $n = 26$; $P < 0.01$). To ensure that there was no bias due to time-dependent effects in these experiments, we additionally compared only experiments where ZD was applied for equal times (ZD time: mHS, 8.2 ± 0.3 min, $n = 9$; sHS, 8.1 ± 0.5 min, $n = 7$; $P = 0.84$). This analysis also resulted in differences of mean ZD-sensitive g_{rest} density (mHS, 14.5 ± 2.4 pS/pF, $n = 9$; sHS, 34.4 ± 7.1 pS/pF, $n = 7$; $P < 0.05$), confirming an increase of I_H in sHS cells. Interestingly, in cells where both conductances were determined subsequently, the Ba^{2+} - and ZD-sensitive g_{rest} correlated ($r = 0.73$, $n = 24$, $P < 0.01$). The relative contribution of the Ba^{2+} -sensitive g_{rest} was on average more enhanced (Ba^{2+} -sensitive/total g_{rest} : mHS, $26.2 \pm 3.1\%$, $n = 15$; sHS, $42.3 \pm 3.2\%$, $n = 13$; $P < 0.01$) than the ZD-sensitive g_{rest} (mHS, $43.1 \pm 4.2\%$, $n = 11$; sHS, $49.4 \pm 2.8\%$, $n = 26$, $P = 0.33$). This result may explain why the initial V_{rest} of sHS cells was slightly hyperpolarized compared with mHS cells (see above). Importantly, both the HCN and Kir conductance correlated with R_{in} in a hyperbolic manner in the pooled cell population (Fig. 1G)

(Ba^{2+} -sensitive g_{rest} and R_{in} : $r = -0.89$, $n = 26$, $P < 0.01$; ZD-sensitive g_{rest} and R_{in} : $r = -0.74$, $n = 37$, $P < 0.01$). In summary, these data indicate that both HCN and Kir channels contribute to the resting conductance of human granule cells, and both conductances were increased in TLE patients with severe hippocampal sclerosis.

Distribution of HCN1 and Kir2.2 Channels in the Hippocampus of TLE Patients

As the main HCN subunit candidate in granule cells is HCN1 (Bender et al. 2003; Notomi and Shigemoto 2004), and large parts of granule cell Kir currents are likely to be mediated by Kir2 channels (see above) (Young et al. 2009), we performed immunocytochemistry experiments using anti-HCN1 channel antibodies and anti-Kir2.2 antibodies in thin paraffin-embedded sections of mHS and sHS sections (Fig. 2). The aim of this analysis was to obtain additional information about the precise somatodendritic distribution of HCN1, and one representative of the Kir2 family, in the human hippocampus. Omitting primary antibodies or replacing them by other IgGs with no hippocampal targets resulted in no staining at all (not shown), confirming antibody specificity. Staining of adjacent sections

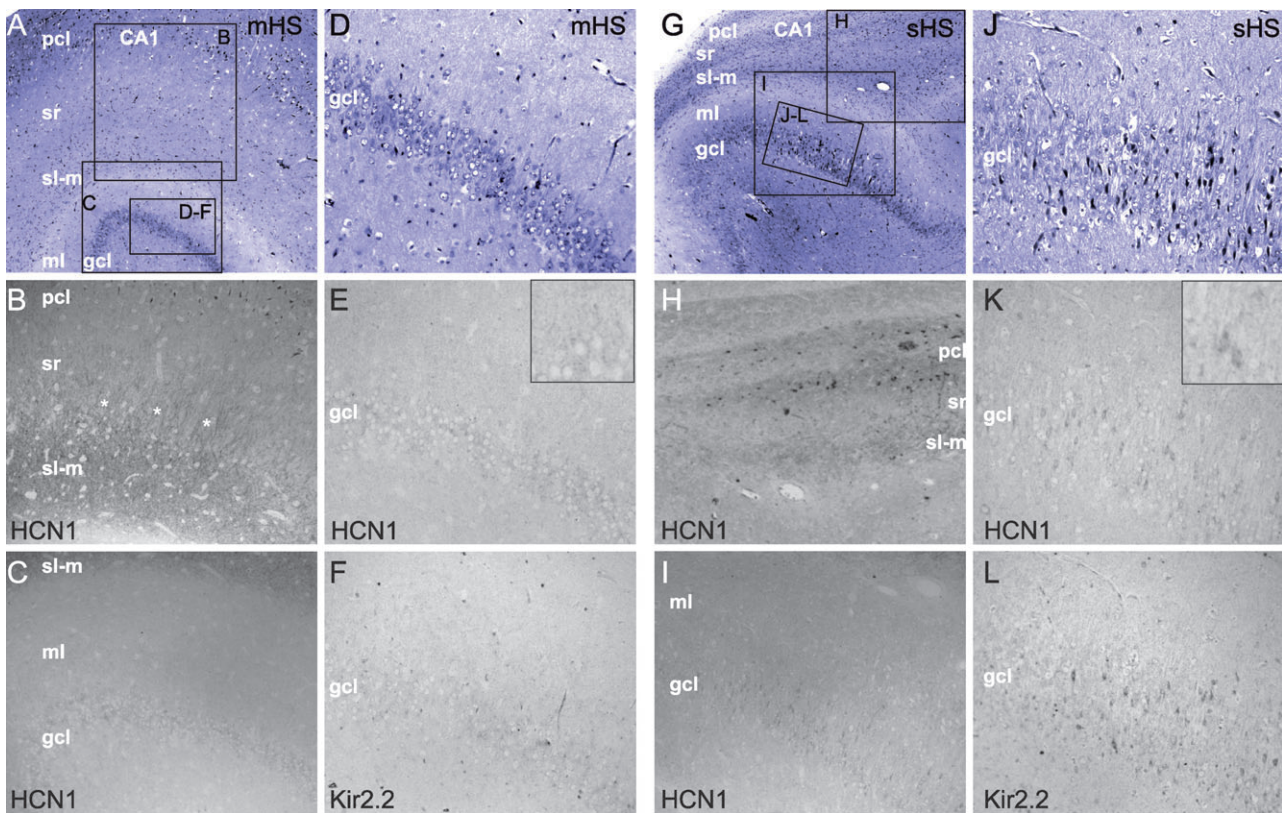


Figure 2. Nissl staining (A, D, G, J), and HCN1 (B, C, E, H, I, K) and Kir2.2 (F, L) immunoperoxidase cytochemistry in hippocampi from TLE patients with mild hippocampal sclerosis (mHS, A–F) and severe hippocampal sclerosis (sHS, G–L). gcl, granule cell layer; ml, molecular layer; pcl, pyramidal cell layer; sr, stratum radiatum; sl-m, stratum lacunosum-moleculare. (A, G) Overview of a Nissl (cresyl violet) stained section displaying regions of the CA1 area and the dentate gyrus. Boxes indicate regions magnified in panels B–F (A) and H–L (G), respectively. Note that in the sHS section (G), pyramidal cells are absent in the CA1 area (except for a small region in the upper right corner). (B, H) At higher magnification, the CA1 region displayed strong HCN1 immunoreactivity of distal pyramidal cell dendrites in the sr (asterisks) and the sl-m of mHS sections (B). In contrast, little HCN1 immunoreactivity is present in the CA1 of sHS sections, presumably due to the loss of pyramidal cells (H). (C, I) At higher magnification, the dentate gyrus with gcl, and ml, showed HCN1 immunoreactivity which was weak compared with the sl-m of the CA1 area but clearly present. Despite reduced cell density, HCN1 staining appeared more intense in the sHS (I) compared with the mHS case (C). (D, J) Higher magnification of the Nissl-stained sections displayed a narrow gcl in the mHS case (D) and a largely dispersed gcl with more dysplastic dark cells in the sHS case (J). (E, K) At the same magnification of the gcl as in D and J (and further magnification in insets), it is evident that not only somata but also proximal dendrites of granule cells display HCN1 immunoreactivity. In contrast to the mHS gcl, in the sHS case, many granule cells are intensely labeled with anti-HCN1 antibodies. (F, L) Similar to the HCN1 staining in the gcl, Kir2.2 immunostaining is present in the gcl of mHS section (F) but intensely labeled granule cells appear only in the sHS case (L).

with cresyl violet showed that sHS sections displayed massive cell loss in CA regions, which was associated with the dispersion of the granule cell layer (Fig. 2 compare *D_i*) as has been described before (Thom et al. 2002).

In mHS sections, HCN1 protein was most abundant in the stratum lacunosum-moleculare (sl-m) of the hippocampal CA1 region. Radial elongated structures in the stratum radiatum (sr), representing distal dendrites of CA1 pyramidal cells, displayed comparably strong HCN1 immunoreactivity (Fig. 2*B*). In comparison, the dentate gyrus displayed lower HCN1-immunoreactivity (Fig. 2*C*). However, in the narrow granule cell layer of the mHS sections, somata clearly express the HCN1 channel protein (Fig. 2*E*, inset). Similarly, the labeling for Kir2.2 protein was weak but detectable in the granule cell layer of mHS patients (Fig. 2*F*).

In sHS sections, HCN1 labeling was reduced in the CA1 region (Fig. 2*H*) compared with mHS cases (Fig. 2*B*), which is likely due to the lack of pyramidal cells and their dendrites in the severely affected hippocampus (Fig. 2*G*). The few remaining pyramidal cells in the CA1 region correspond to sparse HCN1 labeling in the sr and sl-m (Fig. 2*H*). In contrast, the HCN1 staining in the dentate gyrus was not only clearly present in sHS sections but appeared to be increased despite a lower cell density (Fig. 2*I*) compared with mHS sections (Fig. 2*C*). In particular, dysplastic granule cells showed intense HCN1 staining but also dendrites emerging from granule cells with normal appearance were prominently labeled in the sHS sections (Fig. 2*K*). Similarly, the staining for Kir2.2 appeared more intense in the granule cell layer of the sHS sections (Fig. 2*L*) compared with the mHS specimen (Fig. 2*F*).

In summary, these data suggest that HCN1 channels display a similar distribution in the human hippocampus as in the rodent (Notomi and Shigemoto 2004). While in CA1 pyramidal cells, HCN1 protein is concentrated in distal dendrites, in the dentate gyrus, it expressed rather homogeneously. Although true quantification is not possible with immunoperoxidase stainings, the HCN1 and Kir2.2 labeling of granule cells appeared more intense in the dentate gyrus of sHS compared with mHS sections.

Biophysical Characterization of I_H in Human Granule Cells

As the I_H of granule cells had not been systematically analyzed before and as I_H properties could indicate differences in the mediating HCN subunits (Stieber et al. 2005), we characterized the biophysical properties of ZD-sensitive currents (Fig. 3). To reduce the influence of other currents, these voltage-clamp experiments were performed in PTX, CNQX, AP-5, TTX, and 200 μ M Ba^{2+} (Fig. 3*A*). Consistent with the g_{rest} results above, the mean (ZD-sensitive) I_H evoked by larger hyperpolarizations was increased in cells from sHS compared with mHS tissue (Fig. 3*B*) (I_H at -130 mV: mHS, -1.10 ± 0.11 pA/pF, $n = 23$; sHS, -2.27 ± 0.25 pA/pF, $n = 31$, $P < 0.001$). However, the voltage dependence of activation was not different in mHS versus sHS cells (mHS: $V_{50,HCN}$, -75.8 ± 1.2 mV, k_{HCN} , -7.4 ± 1.2 mV, $n = 9$; sHS: $V_{50,HCN}$, -74.7 ± 0.7 mV, k_{HCN} , -6.5 ± 0.7 mV, $n = 7$; $P = 0.54$). Therefore, the cells were pooled for this characterization (Fig. 3*C*) ($V_{50,HCN}$, -75.3 ± 0.9 mV, k_{HCN} , -7.1 ± 0.9 mV, $n = 16$).

The kinetics of I_H activation displayed a fast and a slow time constant, which were in a similar range in mHS and sHS cells (Fig. 3*B*, *Da*, *Db*) (fast τ_{act} at -130 mV: mHS, 18 ± 7 ms, $n = 7$; sHS, 31 ± 3 ms, $n = 7$, $P = 0.11$; slow τ_{act} : mHS, 99 ± 16 ms, $n = 5$,

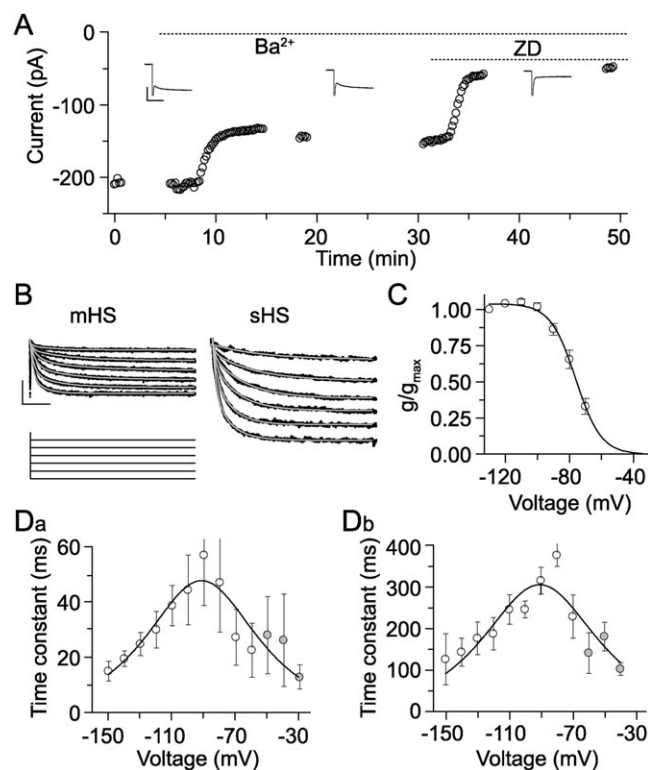


Figure 3. Biophysical characterization of I_H in human granule cells. (A) Inward currents of granule cells evoked by a voltage step from -60 mV to -100 mV were strongly reduced by 200μ M Ba^{2+} and 50μ M ZD7288 (ZD). Insets show examples of respective currents (scale bars, 100 pA, 0.2 s). During steady states, the protocol was paused (hence absence of data points). (B) ZD-sensitive currents (I_H , obtained by subtraction) of mHS and sHS granule cells evoked by the protocol shown below (voltage-clamp steps, 10 mV, from -60 to -130 mV). Scale bars, 50 pA, 250 ms; gray fits, see *D*. (C) The voltage dependence of ZD-sensitive steady state currents (normalized from currents as in *B*) was fitted with a V_{50} value of -75.3 ± 0.9 mV (see Materials and Methods and Results). (D) Fast (*Da*) and slow (*Db*) time constants of activation of I_H (obtained as in *B*). For the complete fit of gating kinetics, time constants of deactivation were included (filled gray circles) (see Materials and Methods, $n = 12$).

sHS, 241 ± 61 ms, $n = 6$, $P = 0.07$). The voltage dependence of the time constants was fitted as shown in Figure 3*D* (see Materials and Methods, fast τ_{act} , $a = 0.48 \pm 0.15$ s $^{-1}$, $b = 231.2 \pm 54.5$ s $^{-1}$, $V_0 = 29.7 \pm 2.5$ mV, $n = 13$; slow τ_{act} , $a = 0.091 \pm 0.041$ s $^{-1}$, $b = 29.5 \pm 10.5$ s $^{-1}$, $V_0 = 31.4 \pm 4.2$ mV, $n = 12$). The amplitude ratio of these time constants was slightly, though not significantly, shifted toward the fast component in the sHS group (amplitude of fast τ_{act} : mHS 61 ± 15 pA, $n = 7$; sHS, 118 ± 30 pA, $n = 7$, $P = 0.12$). The estimated reversal potential of ZD-sensitive currents was -41.9 mV ($n = 10$) resulting in a cation permeability Na^+/K^+ ratio of 0.18 (see Materials and Methods). In summary, these I_H properties are consistent with HCN channels (in particular HCN1), previously characterized in other cell types (Gasparini and DiFrancesco 1997; Franz et al. 2000; Moroni et al. 2000; Santoro et al. 2000; Aponte et al. 2006).

Influence of I_H on the Excitability and Subthreshold Input Integration of Human Granule Cells

The influence of I_H on neuronal excitability is not straightforward: on the one hand, the cation current depolarizes the membrane from its resting potential (V_{rest}), but on the other

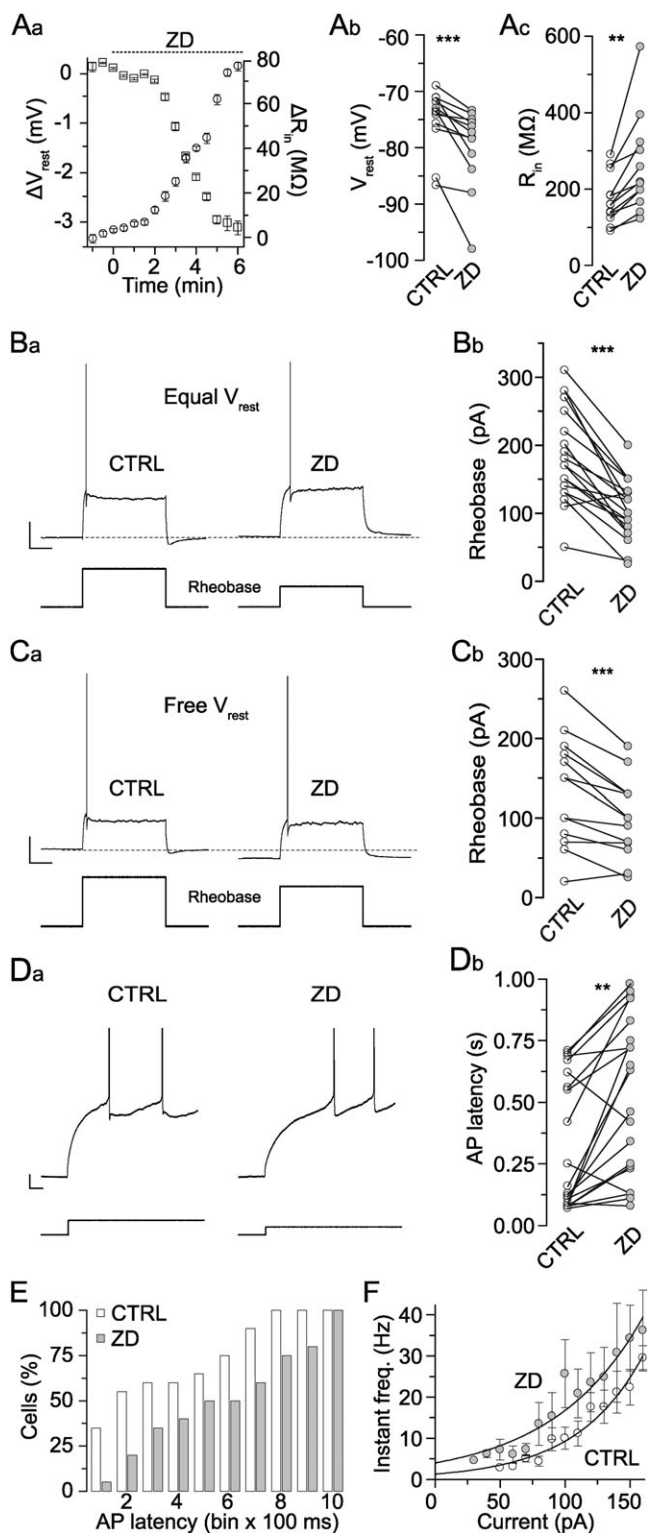


Figure 4. Influence of I_H on the excitability of human granule cells. (A) Effect of I_H inhibitor ZD7288 (ZD, 50 μ M) on the resting membrane potential (V_{rest} , Aa, left y-axis and Ab, $n = 13$) and input resistance (R_{in} , Aa, right y-axis and Ac, $n = 12$). During application of ZD, the R_{in} increased (Ac), while the V_{rest} hyperpolarized (Ab) in parallel. (B, C) Inhibition of I_H via ZD reduced the current necessary to evoke at least one action potential (AP), the “Rheobase,” relative to control (CTRL). This rheobase reduction was visible if the V_{rest} -shift was compensated (Ba, Bb, Equal V_{rest}), and if it was not compensated (Ca, Cb, Free V_{rest}). Thus, despite hyperpolarization by ZD, I_H block increased granule cell excitability. Current steps depicted below: 280 pA (Ba), 150 pA (Bb), 160 pA (Ca), 140 pA (Cb); Scale bars, 20 mV, 0.5 s. (D) The latency of

the first AP with adjusted rheobase injection (see above) was increased when I_H was inhibited. Scale bars, 5 mV, 50 ms. Current steps, 130 pA, 70 pA. (E) With rheobase injection, more than 50% of the cells responded within the first 200 ms under control condition (white bars, $n = 20$), while with ZD only 20% of the cells fired within this period (gray bars, $n = 12$). (F) Instant AP frequency (1/first AP interval) plotted against injected current. I_H inhibition via ZD shifts the response curve to lower input values without changing its form (CTRL, $n = 12$; ZD, $n = 14$, equal V_{rest}). Note that the shift of the response curve is of approximately similar amplitude as the shift in rheobase (Cb).

hand, a large I_H has a shunting influence and is thereby “inhibitory” (Gasparini and DiFrancesco 1997; Dyhrfeld-Johnsen et al. 2009). We explored those functional options for human granule cells (Fig. 4) (pooling mHS and sHS cells). These experiments were conducted in the presence of synaptic inhibitors. Application of ZD hyperpolarized the membrane of granule cells by -4.7 ± 1.1 mV (Fig. 4Aa,Ab) (V_{rest} : control, -75.0 ± 1.5 mV; ZD, -79.6 ± 1.9 mV, $n = 13$, $P < 0.001$). Simultaneous with ZD-mediated hyperpolarization, the R_{in} increased (Fig. 4Aa,Ac) (by 84.4 ± 21.1 M Ω ; R_{in} : control, 179.3 ± 18.7 M Ω ; ZD, 263.7 ± 36.2 M Ω , $n = 12$, $P < 0.01$). These results demonstrate that HCN channels contribute to the regulation of V_{rest} in human granule cells.

To assess the net contribution of I_H on granule cell excitability, the minimal current necessary to trigger at least one action potential (rheobase) was measured. We first analyzed the influence of I_H independent of its effect on V_{rest} by compensating the hyperpolarization during ZD application (V_{rest} : control, -84.4 ± 0.5 mV; ZD, -84.1 ± 0.5 mV, $n = 20$ [7 mHS, 13 sHS], $P = 0.21$). With this, ZD reduced the rheobase strongly (Fig. 4Ba,Bb) (equal V_{rest} rheobase: control, 188 ± 15 pA; ZD, 107 ± 10 pA, $n = 20$, $P < 0.001$), that is, a reduction by 43%. To test the influence of I_H including its effect on V_{rest} , the rheobase was measured with V_{rest} that was left free to change (Fig. 4C). Despite the hyperpolarization by ZD, the rheobase was again decreased after ZD application (Fig. 4Ca,Cb) (free V_{rest} rheobase: control, 134 ± 19 pA; ZD, 100 ± 14 pA, $n = 13$ [5 mHS, 8 sHS], $P < 0.001$). Thus, the net influence of I_H in human granule cells was rather inhibition by shunting than excitation by depolarization. Indeed, the rheobase (free V_{rest}) correlated with the ZD-sensitive g_{rest} ($r = 0.40$, $n = 36$, $P < 0.05$).

Next, we determined the influence of I_H on the action potential response properties of granule cells. Since ZD reduced the rheobase, we compared the latency of the first action potential at rheobase injection. The response latency was prolonged during ZD application (Fig. 4Da,Db) (AP latency: control, 0.31 ± 0.06 s; ZD, 0.52 ± 0.07 s, $n = 20$, $P < 0.01$), consistent with a rebound effect of the I_H (Pape 1996). This suggests that I_H can accelerate the responses. Indeed, more than 50% of the cells fired within the first 200 ms under control conditions, while during ZD application only 20% of the cells responded in this period with rheobase stimulation (Fig. 4E).

In addition, we tested the effect of ZD on the instantaneous action potential frequency (1/first interspike interval). Inhibition of I_H led to an increase of the instant frequency with a given current injection, shifting the current-frequency curve to lower input current values ($P < 0.001$), without changing the shape of the curve (Fig. 4F). Interestingly, the shift of the response curve by approximately 50 pA corresponds roughly to the range by which ZD reduced the rheobase (Fig. 4Bb). These results suggest that I_H regulates the resting membrane

potential and the subthreshold response properties of granule cells. In addition, I_H is suitable to downscale the excitability of human granule cells and to ensure fast reliable responses.

In CA1 pyramidal cells, I_H produces subthreshold membrane resonance effects by allowing larger voltage deflections in the theta frequency range (2–10 Hz) than at any other frequency (Narayanan and Johnston 2007; Hu et al. 2009). We tested the subthreshold resonance behavior of human granule cells using injections of small sinusoidal currents with increasing frequency and we calculated the impedance profiles (Fig. 5) (see Materials and Methods). These experiments were conducted in the presence of synaptic inhibitors. The effects were not different in mHS and sHS cells, and the results were pooled ($n = 3$ and 9, respectively). Granule cells showed low-pass filter behavior typical for biological membranes; under control conditions, the voltage responses and the resulting impedance showed decreasing amplitudes with increasing input frequency (Fig. 5Aa,Ab). Resonance in the impedance profile was quantified by the Q value (see Materials and Methods) (Hu et al. 2009). The Q values were close to one, indicating no resonance (Q value: 1.01 ± 0.005 , $n = 12$). During application of 200 μM Ba^{2+} , the voltage and impedance amplitudes increased but no peak at frequencies higher than 1 Hz could be detected (Fig. 5Ab). After the additional application of ZD, the voltage responses and impedance further increased, in particular at frequencies below ~ 8 Hz. However, no specific peak was revealed by ZD application (Fig. 5Ab). We have tested these experiments at different membrane potentials, frequencies, and temperatures (not shown) but were unable to detect any discernable resonance peak. Therefore, we conclude that I_H does not play a prominent role for membrane resonance in granule cells (see also simulations below).

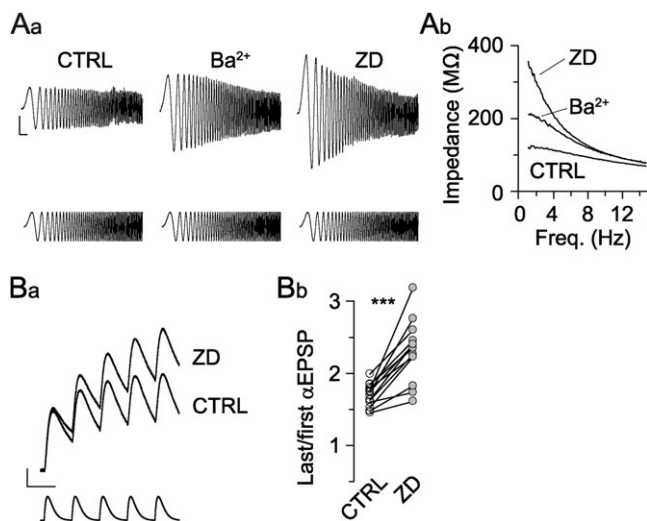


Figure 5. Influence of I_H inhibitor ZD7288 (ZD, 50 μM) on the subthreshold membrane properties of human granule cells. (A) Test of membrane resonance. Injection of small (100 pA) sinusoidal currents with increasing frequency (Aa, lower traces), led to voltage responses (Aa, upper traces) which had decreasing amplitudes with increasing input frequency at control conditions (CTRL). This low-pass filter property was enhanced with 200 μM Ba^{2+} and further increased with additional application of ZD (Aa). The resulting impedance profile showed no specific resonance peak (Ab). Starting membrane potential -90 mV. Scale bars, 10 mV, 1 s. (B) Subthreshold integration of artificial synaptic inputs. Injection of a 50 Hz αEPSC train (Ba, lower trace) evoked EPSPs which leveled off quickly under control conditions but accumulated almost linearly when I_H was blocked (ZD). Thus, I_H decreases the summation (Bb, ratio of last and first EPSP; $n = 13$). Scale bars, 2 mV, 20 ms.

To assess the role of HCN channels in subthreshold integration of synaptic inputs, we applied a train of 5 artificial αEPSCs at 50 Hz and measured the summation of evoked potentials (αEPSPs). Before application of ZD, αEPSPs accumulated and leveled off at a low intensity of depolarization (Fig. 5Ba). In contrast, following ZD application αEPSPs added up more quickly to higher depolarizations and did not saturate in the tested time (Fig. 5Ba). Thus, inhibition of I_H increased the summation of αEPSPs by 35% (Fig. 5Bb) (last/first αEPSP : control, 1.70 ± 0.04 ; ZD, 2.31 ± 0.12 , $n = 13$ [4 mHS, 9 sHS]; $P < 0.001$). These results suggest that I_H effectively attenuates the impact of EPSPs (see also simulations below).

Influence of Kir Currents on the Excitability and Subthreshold Input Integration of Human Granule Cells

The results above and previous data (Stegen et al. 2009; Young et al. 2009) suggest that granule cells of sHS sections possess more Kir conductances than control granule cells. Therefore, we investigated the effect of Kir conductances on the rheobase and αEPSCs (Fig. 6) as described for the I_H above. Application of 200 μM Ba^{2+} depolarized the membrane, which was compensated to approximately -85 mV, and reduced the rheobase (Fig. 6Aa,Ab) (control, 116 ± 18 pA; Ba^{2+} , 78 ± 10 pA, $n = 11$, $P < 0.01$). This effect was expected: blocking the large K^+ conductance of granule cells increases their excitability. However, it was surprising, that the shunting effect of Kir (33%) was smaller than the shunting effect of I_H (43%, see above).

Similarly, it was expected that Kir inhibition decreased the subthreshold summation of αEPSCs (Fig. 6Ba,Bb) (last/first αEPSP : control, 1.93 ± 0.08 ; Ba^{2+} , 2.45 ± 0.15 , $n = 8$, $P < 0.01$). However, it was notable that this effect (27%) was not bigger

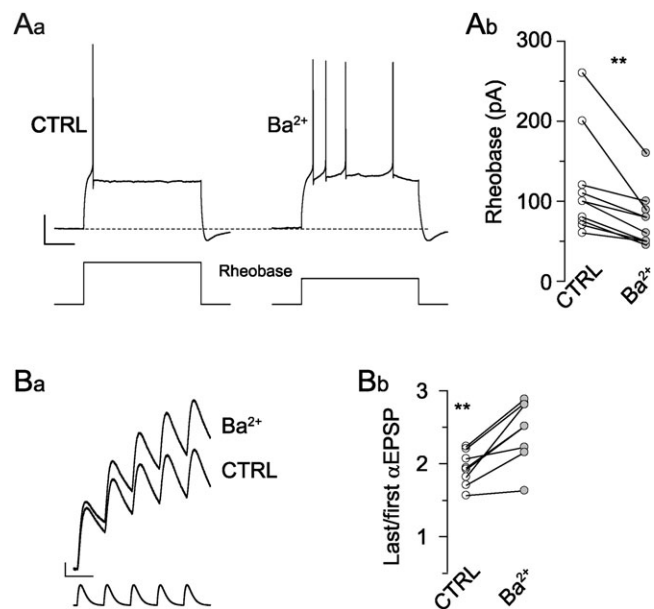


Figure 6. (A) Influence of 200 μM Ba^{2+} -sensitive (Kir) conductances on the current necessary to evoke at least one action potential (Rheobase) in human granule cells. Inhibition of Kir conductances reduced the rheobase. Note that the effect of Ba^{2+} was in a similar range as the effect of ZD (Fig. 4B, V_{rest} corrected). Current-clamp steps below, 260 pA, 160 pA (Aa). Scale bars, 20 mV, 0.5 s ($n = 11$). (B) Influence of 200 μM Ba^{2+} on subthreshold integration of artificial synaptic inputs (5 αEPSCs of 150 pA, at 50 Hz, $n = 8$). The summation of evoked EPSPs was reduced by Kir inhibition (Ba^{2+}). Note that the effect of Ba^{2+} was again in a similar range as the effect of ZD (Fig. 5B). Scale bars, 2 mV, 20 ms.

than the α EPSP attenuation by I_H (35%). In summary, these results demonstrate that the HCN conductance has a shunting influence with approximately equal impact on granule cell excitability and input summation, as the Kir conductance.

Granule Cell Excitability in Sections with mHS and sHS

As the above results suggested that greater I_H and Kir conductances in sHS granule cells resulted in strong shunting, it would be expected that sHS cells are less excitable than mHS cells (Fig. 7). Indeed, the rheobase of sHS cells was increased compared with mHS cells (Fig. 7Aa,Ab) (rheobase: mHS, 84 ± 11 pA, $n = 37$; sHS, 129 ± 10 pA, $n = 49$; $P < 0.001$). Normalized to cell capacitance, this difference remained (rheobase density: mHS, 0.83 ± 0.10 pA/pF, $n = 37$; sHS, 1.49 ± 0.16 pA/pF, $n = 49$; $P < 0.001$). Overall, the rheobase correlated with the R_{in} of granule cells (Fig. 7B) ($r = 0.75$, $n = 86$; $P < 0.01$).

Furthermore, the above ZD results suggest that I_H accelerates responses and shifts the current–frequency curve. Therefore, we compared these properties in mHS and sHS cells. On average, the action potential latencies analyzed at rheobase current injections were slightly, but not significantly, reduced in sHS cells (Fig. 7C) (mHS, 0.47 ± 0.10 s, $n = 7$; sHS, 0.23 ± 0.06 s, $n = 13$; $P = 0.057$). However, when analyzing the physiologically more relevant first part of the 1-s response, sHS cells responded more often within the first 200 ms compared with mHS cells (Fig. 7C) (mHS, 53%; sHS, 69%). Analyzing the instant frequency (see above), the input–output curve of sHS cells was shifted to higher input currents ($P < 0.001$) (Fig. 7D). In agreement to the effect of ZD, this shift of the response curve by approximately 50 pA (Fig. 7D) corresponds roughly to the value by which the rheobase of sHS cells was increased (Fig. 7Ab). Thus, assuming the input strength would increase by 50 pA from mHS to sHS, an I_H upregulation as observed (Fig. 7D) would produce a response with similar instant frequency in the sHS cells as in the mHS cells. These results indicate that the upregulation of I_H in sHS cells is suitable to conserve the output characteristics with increased input strengths.

It has been shown that granule cells receive increased excitatory input in TLE animal models (Wuarin and Dudek 2001). Consistent with this hypothesis, spontaneous EPSCs were indeed enlarged in sHS cells (not shown, charge transfer: mHS, 83.8 ± 10.9 fC/pF, $n = 7$; sHS, 140.1 ± 16.1 fC/pF, $n = 17$, $P < 0.05$).

Our results imply that the reduced R_{in} of granule cells is related to the severity of hippocampal destruction during TLE. As the latter is related to the epileptic seizures, a logical question would be: does granule cell R_{in} correlate with the amount of seizures? To address this question, we pooled all R_{in} values from this and a previous study on human granule cells (Stegen et al. 2009) and plotted them against the duration of epilepsy reported by the respective patients. Indeed, the R_{in} correlated with the epilepsy duration (Fig. 7Ea) ($r = 0.22$, $n = 139$, $P < 0.01$). This effect could be due to the different ages of the patients. However, arguing against this possibility, the R_{in} did not correlate with the patient's age at surgery (Fig. 7Eb) ($r = 0.11$, $n = 139$, $P = 0.19$). This lack of correlation remained when mHS and sHS cells were analyzed separately (mHS, $r = 0.03$, $n = 52$, $P = 0.8$; sHS, $r = 0.1$, $n = 87$, $P = 0.4$). Although causal conclusions cannot directly be drawn from such a correlation, the combination of results indicates that the upregulation of

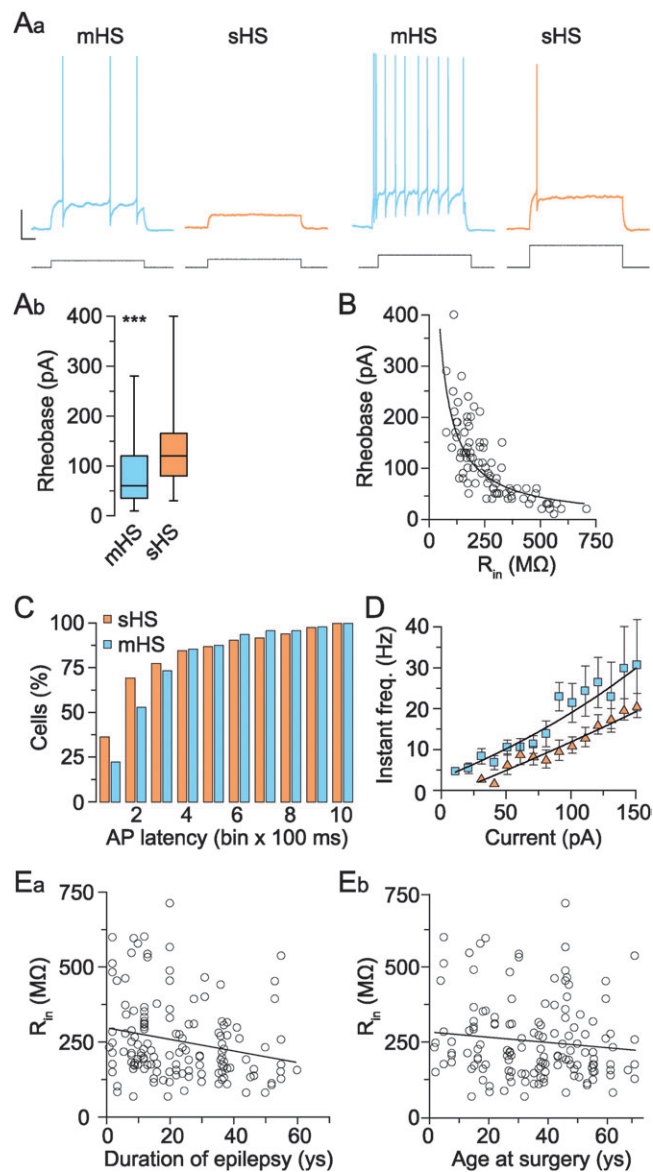


Figure 7. The excitability of granule cells from TLE patients with sHS (orange) was reduced compared with those with mHS (blue). (A) Small currents evoked action potentials (APs) in the mHS but not the sHS cell, and stronger currents evoked massive spiking in the mHS but only one AP in the sHS cell. The minimal current necessary to evoke an AP (Rheobase, Ab) was increased in sHS versus mHS cells ($n = 49$ and 37 , respectively). Current protocols in Aa (black traces below), from left to right, 50, 90, 60, 160 pA, respectively. Scale bars, 20 mV, 0.25 s. (B) The rheobase of pooled granule cells correlated with the R_{in} of respective cells ($n = 86$). (C) With rheobase injection, 53% of mHS cells and 69% of the sHS cells produced an AP within the first 200 ms (blue bars, mHS, $n = 7$; orange bars, sHS, $n = 13$). (D) Plot of instant AP frequency (1/first AP interval) against injected current. The response curve of sHS cells was shifted to higher input values compared with mHS cells ($n = 24$ and 16 , respectively). Note that the shift of the response curve is of approximately similar amplitude as the shift in rheobase (Ab). (E) The R_{in} of pooled granule cells of this and a previous study (Stegen et al. 2009) ($n = 139$, see Results) was reduced in TLE patients with reported duration of epilepsy (Ea) but not with the patient's age at surgery (Eb).

granule cell leak conductances could be an adaptive reaction to increased excitation, possibly related to epileptic seizures.

Computer Simulations of I_H in Human Granule Cells

Why does I_H not produce membrane resonance in granule cells as it does in other cell types? Is it possible to reproduce the

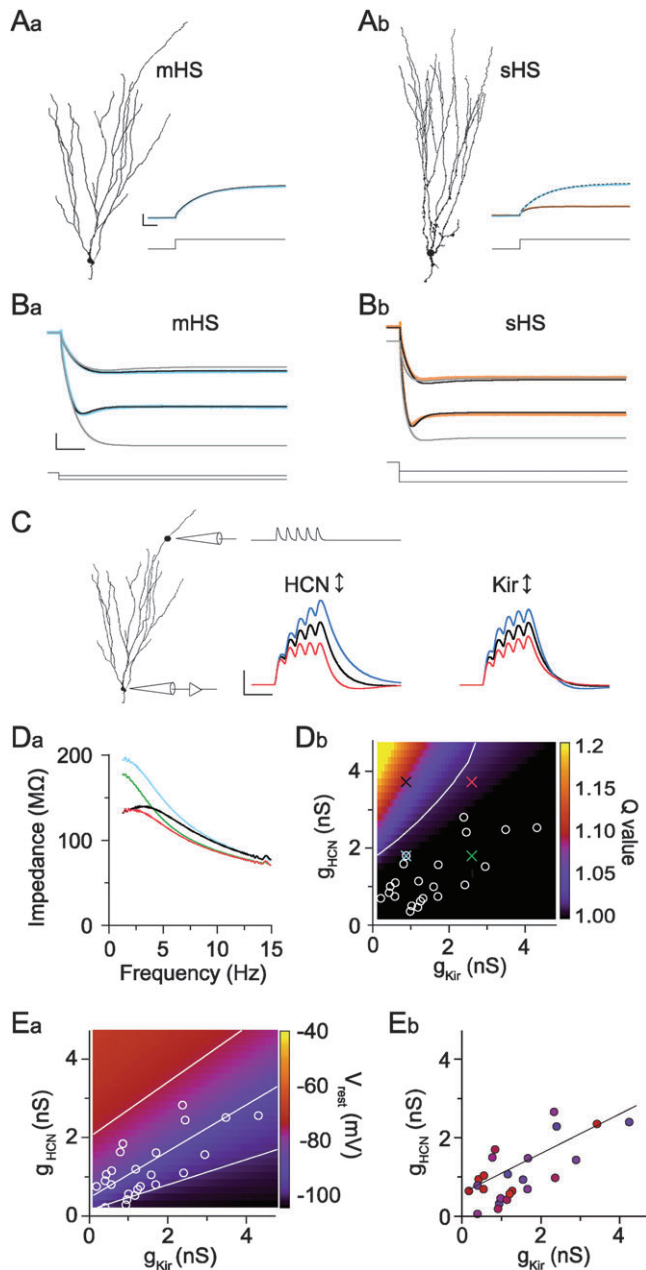


Figure 8. Conductance-based computer models of reconstructed granule cells from TLE patients with different degrees of hippocampal sclerosis (mHS, sHS, respectively). (A) The passive properties were fitted (black traces) to experimentally recorded charging curves of a mHS cell (Aa, blue trace) and a sHS cell (Ab, orange trace). Current steps were 10 pA (lower traces). Implementing the mHS properties (R_a , R_m) in the sHS morphology (corrected for surface difference) resulted in a charging curve identical to the original mHS curve (compare Ab, blue trace and broken line with Aa). Scale bars, 1 mV, 25 ms. (B) The HCN and Kir conductances (g_{HCN} and g_{Kir} , respectively) were implemented in the models (see Materials and Methods). The V_{rest} and “sag” responses of models (Ba, Bb, black lines) were similar to those experimentally recorded in respective cells (blue and orange traces). Without g_{Kir} (replaced by a linear g_{pas}), these responses could not be fitted (Ba, Bb, gray lines). Scale bars, 10 mV, 50 ms. Lower traces, current steps -130 pA, -380 pA (mHS), -400 pA, -1000 pA (sHS). (C) Summation of “synaptic” inputs injected distally (5 α EPSCs of 60 pA, at 50 Hz), with different HCN (left) and Kir (right) densities in the mHS model (black, 100%; blue, 10%; red, 200%, see text). Note that EPSP summation was remarkably reduced in the sHS-like cases (red). Scale bars, 1 mV, 50 ms. (D) Test for membrane resonance in the mHS model with different g_{HCN} and g_{Kir} densities. The impedance-frequency profiles (Da) and their resonances were quantified by the Q value (Db, see Materials and Methods). Resonance only occurred (above $Q = 1.02$, white line), with high g_{HCN} and low g_{Kir} densities

mHS and sHS phenotypes by implementing realistic HCN and Kir conductivities? How does the combined upregulation of Kir and HCN conductances influence the V_{rest} ? To address these questions, we performed computer simulations by constructing conductance-based models from morphologically reconstructed human granule cells (Fig. 8). The passive membrane properties, R_a and R_m were fitted to obtain the charging curves experimentally recorded in the respective cells (Fig. 8Aa, Ab, see Materials and Methods).

To evaluate the influence of cell size and geometry on the R_{in} difference between these cells, we transferred the passive mHS properties (R_a , R_m) to the sHS model. The resulting charging curve was slightly lower than the original mHS curve (not shown) but correction for the surface difference (factor 1.39) yielded a curve identical to the original mHS curve (Fig. 8Ab). Thus, consistent with our experimental results (Fig. 1D), the surface difference was only responsible for a minor part of the R_m difference between these 2 cells but not the marked difference in R_{in} . In addition, these simulations show that variations in cell geometry between these cells (such as ratio of proximal to distal dendritic diameters etc.) were also not responsible for their R_{in} difference.

Next, we additionally implemented an HCN conductance (g_{HCN}) and a Kir conductance (g_{Kir}) into the 2 models (see Materials and Methods). The best fit, reproducing the V_{rest} , R_{in} and sag voltage responses of the real cells, was obtained when g_{Kir} and g_{pas} (and g_{HCN}) were approximately doubled in the sHS model (Fig. 8Ba, Bb). In contrast, if g_{Kir} was replaced by g_{pas} , the voltage responses could not be fitted (Fig. 8Ba, Bb, gray traces). The electrophysiological phenotype of the sHS cell could be reproduced by implementing its HCN and Kir conductances (corrected for the surface difference) into the mHS morphology. These results indicate that the changes in HCN and K^+ conductances could explain the major part of the subthreshold differences between mHS and sHS cells.

We simulated the subthreshold summation of EPSCs in the models by injecting α EPSCs at distal points of the apical dendrite of the mHS and sHS model. The qualitative difference in input summation was similar when α EPSCs were injected in the soma (not shown) or into the distal dendrites (Fig. 8C). To obtain independence of morphological differences, the effects of HCN and Kir conductances were simulated only in the mHS model. If the HCN conductance was set close to zero (10%), α EPSPs summation was increased. Similarly, reducing the Kir conductance to 10% increased the summation. This effect was slightly smaller than with HCN inhibited. Similar to recent observations in rodent granule cells (Krueppel et al. 2011), our model of human granule cells predicts considerable voltage attenuation along the dendritic tree, and this attenuation was further increased in the sHS model. These results suggest that despite the depolarizing influence of I_{H} , its shunting effect on input summation is significant even in comparison with Kir (Fig. 8C).

in Da/Db) but not with sHS-like values (red trace/cross), mHS-like values (blue trace/cross) or low g_{HCN} /high g_{Kir} values (green trace/cross). (E) Dependence of V_{rest} (color) on the ratio of g_{HCN} and g_{Kir} . (Ea) White lines, -75 mV, -90 mV, and -100 mV isopotentials. Open white circles, experimentally measured ZD- (g_{HCN}) and Ba^{2+} -sensitive g_{rest} (g_{Kir}) values. (Eb) Experimentally determined V_{rest} values (color scale as in Ea) of recordings. Note that g_{HCN} and g_{Kir} values correlated (line), while the V_{rest} remained relatively constant.

To investigate why I_H did not produce membrane resonance in the theta frequency range (2–10 Hz) in granule cells unlike pyramidal cell types (Narayanan and Johnston 2007; Hu et al. 2009), we applied ZAP pulse protocols to the mHS model and quantified the impedance (Fig. 8*Da*) with the Q value as a measure of resonance (see Materials and Methods) (Fig. 8*D**b*). With g_{HCN} and g_{Kir} as in the mHS model (g_{HCN}/g_{Kir} , 1.89 nS/0.87 nS at -80 mV), only low-pass filter properties were observed. Similarly, with “sHS-like” conductance increases (g_{HCN}/g_{Kir} , 3.78 nS/1.74 nS) or low g_{HCN} and high g_{Kir} conductances (g_{HCN}/g_{Kir} , 1.89 nS/1.74 nS), no resonance was detected (Fig. 8*D*). Only with high g_{HCN} and low g_{Kir} values (g_{HCN}/g_{Kir} , 3.78 nS/0.87 nS), did a resonance peak appear (Fig. 8*Da*,*D**b*). Qualitatively similar results were obtained with the sHS model (not shown). These results explain why HCN channel expression is not associated with membrane resonance in granule cells.

A characteristic parameter of the granule cell phenotype is their hyperpolarized V_{rest} . We simulated the combined effect of g_{HCN} and g_{Kir} on the V_{rest} in the mHS model (Fig. 8*E*). This simulation predicted that approximately equilibrated g_{HCN} and g_{Kir} levels would be suitable to keep V_{rest} in a constant range (Fig. 8*Ea*). Indeed, our experimental g_{HCN} and g_{Kir} recordings (ZD- and Ba²⁺-sensitive g_{rest} at -80 mV, respectively) fall into the equilibrated conductance band and correlated (Fig. 8*Eb*) ($r = 0.59$, $n = 27$, $P < 0.01$). These results suggest that the combined upregulation of HCN and Kir conductances is ideally suited to combine downscaling of excitability with homeostatic V_{rest} regulation.

Discussion

We showed that the excitability of human granule cells decreases with the degree of HS in TLE patients and the duration of epilepsy due to an elevated resting conductance. The latter is mediated in approximately equal amounts by HCN and Kir conductances, which are doubled in TLE patients with sHS versus mHS. Our results include the first functional description of HCN channels in granule cells and determine mechanisms of intrinsic plasticity allowing granule cells to homeostatically scale their excitability.

The Presence of I_H in Granule Cells

Previous rodent studies had concluded that granule cells expressed no detectable somatic I_H (Stabel et al. 1992; Brauer et al. 2001). In direct comparison with other neurons, rodent granule cells display only a small I_H and almost no “sag” response—the current-clamp signature of HCN channels (Spruston and Johnston 1992; Stabel et al. 1992; Pape 1996; Franz et al. 2000; Bender et al. 2007; Krueppel et al. 2011). However, HCN protein and ZD-sensitive currents are present in rodent granule cells (Brauer et al. 2001; Chevaleyre and Castillo 2002; Mellor et al. 2002; Huang and Hsu 2003; Notomi and Shigemoto 2004). In addition, the presence or absence of a sag response is not a reliable predictor for the presence or absence of functional HCN channels (Aponte et al. 2006; Hemond et al. 2009; Huggenberger et al. 2009).

Our pharmacological data demonstrates that I_H is not only present but prominent in granule cells of TLE patients. The discrepancy in the I_H between rodent granule cells and human granule cells could be due to species differences or the epilepsy. Since healthy human granule cells are not available for patch-clamp recordings, it is difficult to address this question

(Williamson et al. 1993). However, because HCN1 mRNA levels are similar in granule cells of mHS and autopsy sections (Bender et al. 2003), we are inclined to consider mHS close to the physiological situation. If this would be the case, one could directly compare the HCN conductance of human mHS and mouse control granule cells: the I_H is approximately doubled in humans. However, normalization to cell surface and R_{in} (M.S., F.K., J.W., unpublished data) indicates that the functional impact of I_H may in fact be similar in granule cells of humans and mice.

Our functional characterization relied on the specificity of ZD7288 (Gasparini and DiFrancesco 1997), which applies for most cited studies on HCN channel function. Our biophysical analysis provides further evidence that the I_H was indeed mediated by HCN channels. Although we have no exclusive evidence for the subunits mediating the I_H of human granule cells, the depolarized half-activation, the fast time constant of activation, and the previously determined increase in HCN1 of sHS cells, all point to HCN1 as the main functional subunit in somatodendritic membranes of human granule cells (Franz et al. 2000; Bender et al. 2003; Stieber et al. 2005; Aponte et al. 2006). The quantification of HCN channels in rodents also indicates that HCN1 channels are more likely than HCN2 and far more likely than HCN3–4 (Notomi and Shigemoto 2004) (see also below).

The inhomogeneous distribution of HCN channels in CA1 pyramidal cells has received much attention (Magee 1999; Lorincz et al. 2002; Notomi and Shigemoto 2004), but it was unclear whether this applies to humans. Our immunohistochemistry confirms that the HCN1 protein is strongly enriched in the sl-m also in the human hippocampus. For granule cells, our HCN1 labeling verifies the somatodendritic presence but does not indicate an inhomogeneous accumulation of HCN channels in distal dendrites.

The Function of HCN and Kir Channels in Granule Cells and the Changed HCN Expression in Epilepsy

We showed that I_H contributes to the V_{rest} of granule cells. Although I_H was depolarizing, its net effect was a reduction of R_{in} and thereby a reduction in excitability. Thus, granule cells join the ranks with other cell types where I_H has a shunting role (Magee 1999; Berger et al. 2001; Poolos et al. 2002). However, the role of I_H is not equal in all these cell types. One proposed function of I_H expressed in distal dendrites of CA1 pyramidal cells is the support of membrane oscillations around theta frequency (Narayanan and Johnston 2007; Hu et al. 2009; Marcelin et al. 2009). On the other hand, hippocampal theta oscillations are increased in mice lacking HCN1 channels (Nolan et al. 2004), and the function of somatic I_H may be different from the function of I_H in distal dendrites (van Welie et al. 2004; Hemond et al. 2009). We could not reproduce I_H -dependent resonance in granule cells, which may be due to cell-specific differences in I_H kinetics, HCN expression patterns, and the interaction with other intrinsic conductances. Our computer simulations indicated that only the combination of high I_H and low Kir amplitudes (which was not observed experimentally) would support resonance.

We detected more HCN conductance density in sHS compared with mHS granule cells. On a superficial level, our result appears in conflict with studies that have highlighted the downregulation of I_H in various seizure models (Dugladze et al.

2007; Richichi et al. 2008). For example, rats systemically injected with kainate or pilocarpine display decreased expression of HCN1 and HCN2 in CA regions and the entorhinal cortex (Brewster et al. 2002; Shah et al. 2004; Jung et al. 2007, 2010; Powell et al. 2008; Shin et al. 2008; Huang et al. 2009; Marcelin et al. 2009). Also in neocortical cells of epilepsy patients (Wierschke et al. 2010) and in hippocampal interneurons of kainate-injected mice (Dugladze et al. 2007), the I_H is decreased. Only few studies found increases in HCN channels in some areas during epilepsy and often combined with HCN reduction in other areas (Chen et al. 2001; Brewster et al. 2002; Dyhrfeld-Johnsen et al. 2008; Shin et al. 2008). Thus, in many cell types, TLE is linked to a downregulation of I_H . In human granule cells, TLE is associated with an upregulation of I_H . Consistently, the downregulation of I_H in other cell types increases the excitability, while the upregulation of I_H in granule cells decreases their excitability.

As in mouse granule cells of severely sclerotic hippocampi (Young et al. 2009), sHS granule cells of TLE patients displayed upregulation of a Kir conductance. Although Ba^{2+} is an unselective drug and we attempted no molecular identification of the Kir conductance of human granule cells, the sensitivity to μM concentrations of Ba^{2+} , and the inward rectification of this K^+ conductance (Stegen et al. 2009) suggest that it was mediated by members of the Kir2 channel family, but other K^+ conductances may also be involved (Coetzee et al. 1999; Young et al. 2009). Interestingly, instead of I_H , a tonic GABA-A conductance was elevated in granule cells of kainate-injected mice (Young et al. 2009), which we did not observe in human granule cells. The reason for this dissimilarity is currently unclear. From a functional point of view, it is intriguing that in both cases (TLE patients and mouse model), an elevated Kir conductance was accompanied by an increase in a shunting but depolarizing conductance. Our computer simulations indicate that the observed co-scaling of Kir and HCN conductances is ideally suited to keep the V_{rest} constant. Indeed, many intracellular processes are tuned to the cell-specific membrane potential. Therefore, we hypothesize that the "goal" of the increased HCN conductance in human granule cells and the tonic GABA-A currents in mice, is in both cases to homeostatically adjust V_{rest} . Consistent with this hypothesis, in other cell types, HCN, K^+ , and GABA-A conductances can be adapted in variable combinations to achieve homeostatic regulation of neuronal excitability (Brickley et al. 2001; van Welie et al. 2004; Fan et al. 2005; Narayanan and Johnston 2007; Chen et al. 2010).

The causal molecular mechanisms of ion channel changes in TLE patients are mostly unclear (Poolos 2009). Amplification of I_H could be an acute effect of certain anti-epileptic drugs (Poolos et al. 2002; Surges et al. 2003), but we have no indication for a bias in drug treatment before surgery. Instead, it is more probable that excessive activation of glutamate receptors and calcium-dependent processes, similar to those inducing long term synaptic potentiation, led to the increase in I_H (Brauer et al. 2001; Fan et al. 2005; Campanac et al. 2008; Richichi et al. 2008). Downstream of these events, a raise in I_H could be due to an elevated expression of HCN channels or an increased activity of existing HCN channels. Although our HCN1 staining indicated an increase in the sHS tissue, HCN1 immunolabeling in the human dentate was too weak to allow differentiation, similar to previous experiences (Bender et al. 2003). A strong argument for an increased expression of HCN channels comes from the HCN1 mRNA quantification in the

human dentate gyrus of sHS versus mHS tissue (Bender et al. 2003). Nevertheless, it is still possible that I_H was additionally enhanced by a change in HCN or auxiliary subunit composition affecting cAMP sensitivity or phosphorylation state (Surges et al. 2006; Santoro et al. 2009; Jung et al. 2010). The similar voltage dependence of I_H in mHS and sHS cells argues against this possibility but the tendency for faster activation is in favor. Generally, the conductance upregulation could be related to a pathological replay of developmental mechanisms (Brewster et al. 2002; Shin et al. 2008).

We detected a correlation of the granule cell R_{in} with the duration of epilepsy but not with the patient's age. The conclusion that the hyperexcitability associated with seizures could therefore be responsible for the R_{in} changes is obviously speculative. We do not know the actual number of seizures that invaded the hippocampus. Also the degree of HS is no reliable marker for seizure frequency (Cendes et al. 1993; de Lanerolle and Lee 2005). In support of the hypothesis that detected R_{in} changes could nevertheless be due to (perhaps subclinical) excessive activation of granule cells, we detected enhanced excitatory synaptic inputs in sHS cells. Thus, while granule cells are likely externally hyperexcited during TLE (Wuarin and Dudek 2001), accumulating evidence suggests that granule cells intrinsically adapt and eventually become hypoexcitable (present study; Stegen et al. 2009; Young et al. 2009). Despite this gain reduction, human granule cells of TLE patients are still functional: sHS and mHS cells showed a similar initial action potential response when the rheobase difference was compensated. This effect suggests that the granule cell output is homeostatically scaled via the combined regulation of Kir and HCN conductances.

Funding

Deutsche Forschungsgemeinschaft (DFG, SFB780/C2).

Notes

We thank Prof C. A. Haas, Prof J. Zentner, and Prof M. Prinz for infrastructural support, Dr J. Beckervordersandforth for cooperative tissue handling, F. Moos, and H. Heilmann for help with immunocytochemical procedures, C. Schneider and J. Kang for manuscript corrections, and Prof J. Bischofberger for helpful discussion. Computing resources were provided by the Black Forest Grid Initiative, and image processing was performed in the Life Imaging Center Freiburg. *Conflict of Interest:* None declared.

References

- Aponte Y, Lien CC, Reisinger E, Jonas P. 2006. Hyperpolarization-activated cation channels in fast-spiking interneurons of rat hippocampus. *J Physiol.* 574:229–243.
- Bender RA, Kirschstein T, Kretz O, Brewster AL, Richichi C, Ruschenschmidt C, Shigemoto R, Beck H, Frotscher M, Baram TZ. 2007. Localization of HCN1 channels to presynaptic compartments: novel plasticity that may contribute to hippocampal maturation. *J Neurosci.* 27:4697–4706.
- Bender RA, Soleymani SV, Brewster AL, Nguyen ST, Beck H, Mathern GW, Baram TZ. 2003. Enhanced expression of a specific hyperpolarization-activated cyclic nucleotide-gated cation channel (HCN) in surviving dentate gyrus granule cells of human and experimental epileptic hippocampus. *J Neurosci.* 23:6826–6836.
- Berger T, Larkum ME, Luscher HR. 2001. High I(h) channel density in the distal apical dendrite of layer V pyramidal cells increases bidirectional attenuation of EPSPs. *J Neurophysiol.* 85:855–868.
- Brauer AU, Savaskan NE, Kole MH, Plaschke M, Monteggia LM, Nestler EJ, Simburger E, Deisz RA, Ninnemann O, Nitsch R. 2001.

- Molecular and functional analysis of hyperpolarization-activated pacemaker channels in the hippocampus after entorhinal cortex lesion. *FASEB J*. 15:2689-2701.
- Brewster A, Bender RA, Chen Y, Dube C, Eghbal-Ahmadi M, Baram TZ. 2002. Developmental febrile seizures modulate hippocampal gene expression of hyperpolarization-activated channels in an isoform- and cell-specific manner. *J Neurosci*. 22:4591-4599.
- Brickley SG, Revilla V, Cull-Candy SG, Wisden W, Farrant M. 2001. Adaptive regulation of neuronal excitability by a voltage-independent potassium conductance. *Nature*. 409:88-92.
- Campanac E, Daoudal G, Ankri N, Debanne D. 2008. Downregulation of dendritic I(h) in CA1 pyramidal neurons after LTP. *J Neurosci*. 28:8635-8643.
- Cendes F, Andermann F, Gloor P, Lopes-Cendes I, Andermann E, Melanson D, Jones-Gotman M, Robitaille Y, Evans A, Peters T. 1993. Atrophy of mesial structures in patients with temporal lobe epilepsy: cause or consequence of repeated seizures? *Ann Neurol*. 34:795-801.
- Chen K, Aradi I, Thon N, Eghbal-Ahmadi M, Baram TZ, Soltesz I. 2001. Persistently modified h-channels after complex febrile seizures convert the seizure-induced enhancement of inhibition to hyperexcitability. *Nat Med*. 7:331-337.
- Chen X, Shu S, Schwartz LC, Sun C, Kapur J, Bayliss DA. 2010. Homeostatic regulation of synaptic excitability: tonic GABA(A) receptor currents replace I(h) in cortical pyramidal neurons of HCN1 knock-out mice. *J Neurosci*. 30:2611-2622.
- Chevalyere V, Castillo PE. 2002. Assessing the role of Ih channels in synaptic transmission and mossy fiber LTP. *Proc Natl Acad Sci U S A*. 99:9538-9543.
- Coetzee WA, Amarillo Y, Chiu J, Chow A, Lau D, McCormack T, Moreno H, Nadal MS, Ozaita A, Pountney D, et al. 1999. Molecular diversity of K⁺ channels. *Ann N Y Acad Sci*. 868:233-285.
- de Lanerolle NC, Lee TS. 2005. New facets of the neuropathology and molecular profile of human temporal lobe epilepsy. *Epilepsy Behav*. 7:190-203.
- Dugladze T, Vida I, Tort AB, Gross A, Otahal J, Heinemann U, Kopell NJ, Gloveli T. 2007. Impaired hippocampal rhythmogenesis in a mouse model of mesial temporal lobe epilepsy. *Proc Natl Acad Sci U S A*. 104:17530-17535.
- Dyhrfeld-Johnsen J, Morgan RJ, Foldy C, Soltesz I. 2008. Upregulated H-Current in hyperexcitable CA1 dendrites after febrile seizures. *Front Cell Neurosci*. 2:2.
- Dyhrfeld-Johnsen J, Morgan RJ, Soltesz I. 2009. Double trouble? Potential for hyperexcitability following both channelopathic up- and downregulation of I(h) in epilepsy. *Front Neurosci*. 3:25-33.
- Fan Y, Fricker D, Brager DH, Chen X, Lu HC, Chitwood RA, Johnston D. 2005. Activity-dependent decrease of excitability in rat hippocampal neurons through increases in I(h). *Nat Neurosci*. 8:1542-1551.
- Franz O, Liss B, Neu A, Roeper J. 2000. Single-cell mRNA expression of HCN1 correlates with a fast gating phenotype of hyperpolarization-activated cyclic nucleotide-gated ion channels (Ih) in central neurons. *Eur J Neurosci*. 12:2685-2693.
- Gasparini S, DiFrancesco D. 1997. Action of the hyperpolarization-activated current (Ih) blocker ZD 7288 in hippocampal CA1 neurons. *Pflugers Arch*. 435:99-106.
- Hemond P, Migliore M, Ascoli GA, Jaffe DB. 2009. The membrane response of hippocampal CA3b pyramidal neurons near rest: heterogeneity of passive properties and the contribution of hyperpolarization-activated currents. *Neuroscience*. 160:359-370.
- Hsu D. 2007. The dentate gyrus as a filter or gate: a look back and a look ahead. *Prog Brain Res*. 163:601-613.
- Hu H, Vervaeke K, Graham LJ, Storm JF. 2009. Complementary theta resonance filtering by two spatially segregated mechanisms in CA1 hippocampal pyramidal neurons. *J Neurosci*. 29:14472-14483.
- Huang CC, Hsu KS. 2003. Reexamination of the role of hyperpolarization-activated cation channels in short- and long-term plasticity at hippocampal mossy fiber synapses. *Neuropharmacology*. 44:968-981.
- Huang Z, Walker MC, Shah MM. 2009. Loss of dendritic HCN1 subunits enhances cortical excitability and epileptogenesis. *J Neurosci*. 29:10979-10988.
- Huggenberger S, Vater M, Deisz RA. 2009. Interlaminar differences of intrinsic properties of pyramidal neurons in the auditory cortex of mice. *Cereb Cortex*. 19:1008-1018.
- Isokawa M. 1996. Decrement of GABAA receptor-mediated inhibitory postsynaptic currents in dentate granule cells in epileptic hippocampus. *J Neurophysiol*. 75:1901-1908.
- Jung MW, McNaughton BL. 1993. Spatial selectivity of unit activity in the hippocampal granular layer. *Hippocampus*. 3:165-182.
- Jung S, Bullis JB, Lau IH, Jones TD, Warner LN, Poolos NP. 2010. Downregulation of dendritic HCN channel gating in epilepsy is mediated by altered phosphorylation signaling. *J Neurosci*. 30:6678-6688.
- Jung S, Jones TD, Lugo JN Jr, Sheerin AH, Miller JW, D'Ambrosio R, Anderson AE, Poolos NP. 2007. Progressive dendritic HCN channelopathy during epileptogenesis in the rat pilocarpine model of epilepsy. *J Neurosci*. 27:13012-13021.
- Krueppel R, Remy S, Beck H. 2011. Dendritic integration in hippocampal dentate granule cells. *Neuron*. 71:512-528.
- Li X, Ascoli GA. 2006. Computational simulation of the input-output relationship in hippocampal pyramidal cells. *J Comput Neurosci*. 21:191-209.
- Liu M, Pleasure SJ, Collins AE, Noebels JL, Naya FJ, Tsai MJ, Lowenstein DH. 2000. Loss of BETA2/NeuroD leads to malformation of the dentate gyrus and epilepsy. *Proc Natl Acad Sci U S A*. 97:865-870.
- Lorincz A, Notomi T, Tamas G, Shigemoto R, Nusser Z. 2002. Polarized and compartment-dependent distribution of HCN1 in pyramidal cell dendrites. *Nat Neurosci*. 5:1185-1193.
- Magee JC. 1999. Dendritic Ih normalizes temporal summation in hippocampal CA1 neurons. *Nat Neurosci*. 2:508-514.
- Marcelin B, Chauviere L, Becker A, Migliore M, Esclapez M, Bernard C. 2009. h channel-dependent deficit of theta oscillation resonance and phase shift in temporal lobe epilepsy. *Neurobiol Dis*. 33:436-447.
- Mellor J, Nicoll RA, Schmitz D. 2002. Mediation of hippocampal mossy fiber long-term potentiation by presynaptic Ih channels. *Science*. 295:143-147.
- Moroni A, Barbuti A, Altomare C, Viscomi C, Morgan J, Baruscotti M, DiFrancesco D. 2000. Kinetic and ionic properties of the human HCN2 pacemaker channel. *Pflugers Arch*. 439:618-626.
- Narayanan R, Johnston D. 2007. Long-term potentiation in rat hippocampal neurons is accompanied by spatially widespread changes in intrinsic oscillatory dynamics and excitability. *Neuron*. 56:1061-1075.
- Nolan MF, Malleret G, Dudman JT, Buhl DL, Santoro B, Gibbs E, Vronskaya S, Buzsaki G, Siegelbaum SA, Kandel ER, et al. 2004. A behavioral role for dendritic integration: HCN1 channels constrain spatial memory and plasticity at inputs to distal dendrites of CA1 pyramidal neurons. *Cell*. 119:719-732.
- Notomi T, Shigemoto R. 2004. Immunohistochemical localization of Ih channel subunits, HCN1-4, in the rat brain. *J Comp Neurol*. 471:241-276.
- Pape HC. 1996. Queer current and pacemaker: the hyperpolarization-activated cation current in neurons. *Annu Rev Physiol*. 58:299-327.
- Poolos NP. 2009. Genetic loss of HCN1 channels is exciting, but is it epileptic? *Epilepsy Curr*. 10:51-52.
- Poolos NP, Migliore M, Johnston D. 2002. Pharmacological upregulation of h-channels reduces the excitability of pyramidal neuron dendrites. *Nat Neurosci*. 5:767-774.
- Powell KL, Ng C, O'Brien TJ, Xu SH, Williams DA, Foote SJ, Reid CA. 2008. Decreases in HCN mRNA expression in the hippocampus after kindling and status epilepticus in adult rats. *Epilepsia*. 49:1686-1695.
- Pruss H, Wenzel M, Eulitz D, Thomzig A, Karschin A, Veh RW. 2003. Kir2 potassium channels in rat striatum are strategically localized to control basal ganglia function. *Brain Res Mol Brain Res*. 110:203-219.
- Richichi C, Brewster AL, Bender RA, Simeone TA, Zha Q, Yin HZ, Weiss JH, Baram TZ. 2008. Mechanisms of seizure-induced 'transcriptional channelopathy' of hyperpolarization-activated cyclic nucleotide gated (HCN) channels. *Neurobiol Dis*. 29:297-305.
- Rodriguez A, Ehlenberger DB, Dickstein DL, Hof PR, Wearne SL. 2008. Automated three-dimensional detection and shape classification of

- dendritic spines from fluorescence microscopy images. *PLoS One*. 3:e1997.
- Santoro B, Baram TZ. 2003. The multiple personalities of h-channels. *Trends Neurosci*. 26:550-554.
- Santoro B, Chen S, Luthi A, Pavlidis P, Shumyatsky GP, Tibbs GR, Siegelbaum SA. 2000. Molecular and functional heterogeneity of hyperpolarization-activated pacemaker channels in the mouse CNS. *J Neurosci*. 20:5264-5275.
- Santoro B, Lee JY, Englot DJ, Gildersleeve S, Piskorowski RA, Siegelbaum SA, Winawer MR, Blumenfeld H. 2010. Increased seizure severity and seizure-related death in mice lacking HCN1 channels. *Epilepsia*. 51:1624-1627.
- Santoro B, Piskorowski RA, Pian P, Hu L, Liu H, Siegelbaum SA. 2009. TRIP8b splice variants form a family of auxiliary subunits that regulate gating and trafficking of HCN channels in the brain. *Neuron*. 62:802-813.
- Santoro B, Tibbs GR. 1999. The HCN gene family: molecular basis of the hyperpolarization-activated pacemaker channels. *Ann N Y Acad Sci*. 868:741-764.
- Schmidt-Hieber C, Jonas P, Bischofberger J. 2007. Subthreshold dendritic signal processing and coincidence detection in dentate gyrus granule cells. *J Neurosci*. 27:8430-8441.
- Selke K, Muller A, Kukley M, Schramm J, Dietrich D. 2006. Firing pattern and calbindin-D28k content of human epileptic granule cells. *Brain Res*. 1120:191-201.
- Shah MM, Anderson AE, Leung V, Lin X, Johnston D. 2004. Seizure-induced plasticity of h channels in entorhinal cortical layer III pyramidal neurons. *Neuron*. 44:495-508.
- Shin M, Brager D, Jaramillo TC, Johnston D, Chetkovich DM. 2008. Mislocalization of h channel subunits underlies h channelopathy in temporal lobe epilepsy. *Neurobiol Dis*. 32:26-36.
- Spruston N, Johnston D. 1992. Perforated patch-clamp analysis of the passive membrane properties of three classes of hippocampal neurons. *J Neurophysiol*. 67:508-529.
- Stabel J, Ficker E, Heinemann U. 1992. Young CA1 pyramidal cells of rats, but not dentate gyrus granule cells, express a delayed inward rectifying current with properties of IQ. *Neurosci Lett*. 135:231-234.
- Steephen JE, Manchanda R. 2009. Differences in biophysical properties of nucleus accumbens medium spiny neurons emerging from inactivation of inward rectifying potassium currents. *J Comput Neurosci*. 27:453-470.
- Stegen M, Young CC, Haas CA, Zentner J, Wolfart J. 2009. Increased leak conductance in dentate gyrus granule cells of temporal lobe epilepsy patients with Ammon's horn sclerosis. *Epilepsia*. 50:646-653.
- Stieber J, Stockl G, Herrmann S, Hassfurth B, Hofmann F. 2005. Functional expression of the human HCN3 channel. *J Biol Chem*. 280:34635-34643.
- Surges R, Brewster AL, Bender RA, Beck H, Feuerstein TJ, Baram TZ. 2006. Regulated expression of HCN channels and cAMP levels shape the properties of the h current in developing rat hippocampus. *Eur J Neurosci*. 24:94-104.
- Surges R, Freiman TM, Feuerstein TJ. 2003. Gabapentin increases the hyperpolarization-activated cation current Ih in rat CA1 pyramidal cells. *Epilepsia*. 44:150-156.
- Thom M, Sisodiya SM, Beckett A, Martinian L, Lin WR, Harkness W, Mitchell TN, Craig J, Duncan J, Scaravilli F. 2002. Cytoarchitectural abnormalities in hippocampal sclerosis. *J Neuropathol Exp Neurol*. 61:510-519.
- van Welie I, van Hooft JA, Wadman WJ. 2004. Homeostatic scaling of neuronal excitability by synaptic modulation of somatic hyperpolarization-activated Ih channels. *Proc Natl Acad Sci U S A*. 101:5123-5128.
- Vida I. 2009. 'Leaky' neurons in the epileptic hippocampus: should we get excited? *J Physiol*. 587:4127-4128.
- Wierschke S, Lehmann TN, Dehnicke C, Horn P, Nitsch R, Deisz RA. 2010. Hyperpolarization-activated cation currents in human epileptogenic neocortex. *Epilepsia*. 51:404-414.
- Williamson A, Patrylo PR. 2007. Physiological studies of human dentate granule cells. *Prog Brain Res*. 163:183-198.
- Williamson A, Spencer DD, Shepherd GM. 1993. Comparison between the membrane and synaptic properties of human and rodent dentate granule cells. *Brain Res*. 622:194-202.
- Williamson A, Telfeian AE, Spencer DD. 1995. Prolonged GABA responses in dentate granule cells in slices isolated from patients with temporal lobe sclerosis. *J Neurophysiol*. 74:378-387.
- Wuarin JP, Dudek FE. 2001. Excitatory synaptic input to granule cells increases with time after kainate treatment. *J Neurophysiol*. 85:1067-1077.
- Wyler AR, Dohan FC, Schweitzer JB, Berry AD. 1992. A grading system for hippocampal sclerosis. *J Epilepsy*. 5:220-225.
- Young CC, Stegen M, Bernard R, Muller M, Bischofberger J, Veh RW, Haas CA, Wolfart J. 2009. Upregulation of inward rectifier K+ (Kir2) channels in dentate gyrus granule cells in temporal lobe epilepsy. *J Physiol*. 587:4213-4233.